Cretaceous Research 129 (2022) 105018

Contents lists available at ScienceDirect

Cretaceous Research

journal homepage: www.elsevier.com/locate/CretRes

A new paralligatorid (Crocodyliformes, Neosuchia) from the mid-Cretaceous of Jilin Province, northeastern China

Paul Rummy [a, b, c, *], Xiao-Chun Wu [d, **], James M. Clark [e], Qi Zhao [a, b], Chang-Zhu Jin [a, b], Masateru Shibata [f, g], Feng Jin [h, i, j], Xing Xu [a, b, c]

[a] Key Laboratory of Vertebrate Evolution and Human Origins, Institute of Vertebrate Paleontology and Paleoanthropology, Chinese Academy of Sciences, Beijing, 100044, People's Republic of China
[b] CAS Center for Excellence in Life and Paleoenvironment, Beijing, 100044, People's Republic of China
[c] College of Earth and Planetary Sciences, University of Chinese Academy of Sciences, Beijing, 100049, People's Republic of China
[d] Canadian Museum of Nature, Ottawa, ON K1P 6P4, Canada
[e] The George Washington University, Washington D.C, 20052, USA
[f] Institute of Dinosaur Research, Fukui Prefectural University, Fukui, 910-1195, Japan
[g] Fukui Prefectural Dinosaur Museum, Fukui, 911-8601, Japan
[h] Yanji Municipal Bureau of Land and Resources, Yanji, 133001, People's Republic of China
[i] Yanji Paleontological Research Centre, Yanji, 133001, People's Republic of China
[j] Yanji Dinosaur Museum, Yanji, 133001, People's Republic of China

ARTICLE INFO

Article history:
Received 25 December 2020
Received in revised form
8 August 2021
Accepted in revised form 26 August 2021
Available online 2 September 2021

Keywords:
China
Cretaceous
Crocodyliformes
Neosuchia
Paralligatoridae

ABSTRACT

Numerous dinosaurian, crocodyliform, and testudine fossils have been recently recovered from the mid-Cretaceous of the Yanji Basin, Jilin Province, China. Among the crocodyliform remains, the specimen (YJDM 00009) described here represents a new genus and new species, *Yanjisuchus longshanensis* gen. et sp. nov. It is the third Cretaceous crocodyliform found in Jilin Province after *Paralligator sungaricus* and *Rugosuchus nonganensis*. *Y. longshanensis* is a medium-to-large neosuchian characterized mainly by the frontal with a wedge-shaped elevation anteriorly, a transversely oriented, grooved preorbital ridge, the fused dentaries, and the dentary dentition with a diastema. *Y. longshanensis* was situated phylogenetically within the Paralligatoridae, with *Rugosuchus nonganensis* and many other species of *Paralligator* from Central Asia. The discovery of *Y. longshanensis* not only adds a new group to the local reptilian fauna but also is important to our understanding of the biogeography and diversity of Paralligatoridae in Asia.

1. Introduction

Since the mid-1980s, the Yanji Basin, especially of those from the Tongfosi, Dalazi and Longjing Formations has yielded numerous vertebrate fossils of various kinds and dinosaur tracks in the Cretaceous strata (Zhang, 1986; Tao and Zhang, 1990; Matsukawa et al., 1995, Zhang, 1997; Zhao et al., 2013; Li et al., 2016; Teng and Li, 2017; Xing et al., 2017; Zheng et al., 2021). The basin is an important source of Cretaceous vertebrates in northeastern China (Fig. 1). Geologically, the Yanji Basin is of particular interest as studies have shown its importance as potentially including the Albian-Cenomanian boundary which are rich in resources (Zhong et al., 2020; Shen et al., 2021). It was mentioned that the unconformity between both the Dalazi and Longjing Formation may constitute syn-rift and post-rift stages in the basin (Shen et al., 2021). The basin stretches 50 km north-south and 55 km east-west, reaching a total area of 1670 km^2 in Yanji and Longjing municipalities and the Yanbian Korean Autonomous Prefecture, Jilin Province (Shi, 2008).

A number of Cretaceous crocodyliforms have been found in China including *Paralligator sungaricus* (Sun, 1958), *Edentosuchus tienshanensis* (Pol et al., 2004), *Shantungosuchus hangjinensis* (Wu et al., 1994), *Chimaerasuchus paradoxus* (Wu and Sues, 1996a), and *Rugosuchus nonganensis* (Wu et al., 2001a). Additionally, several teeth from the Cretaceous strata of Changji, Xinjiang and Chia-Yü-

* Corresponding author. Key Laboratory of Vertebrate Evolution and Human Origins, Institute of Vertebrate Paleontology and Paleoanthropology, Chinese Academy of Sciences, Beijing 100044, People's Republic of China.
** Corresponding author. Canadian Museum of Nature, Ottawa, ON K1P 6P4, Canada.
E-mail addresses: paulrummy@ivpp.ac.cn (P. Rummy), xcwu@nature.ca (X.-C. Wu).

https://doi.org/10.1016/j.cretres.2021.105018
0195-6671/

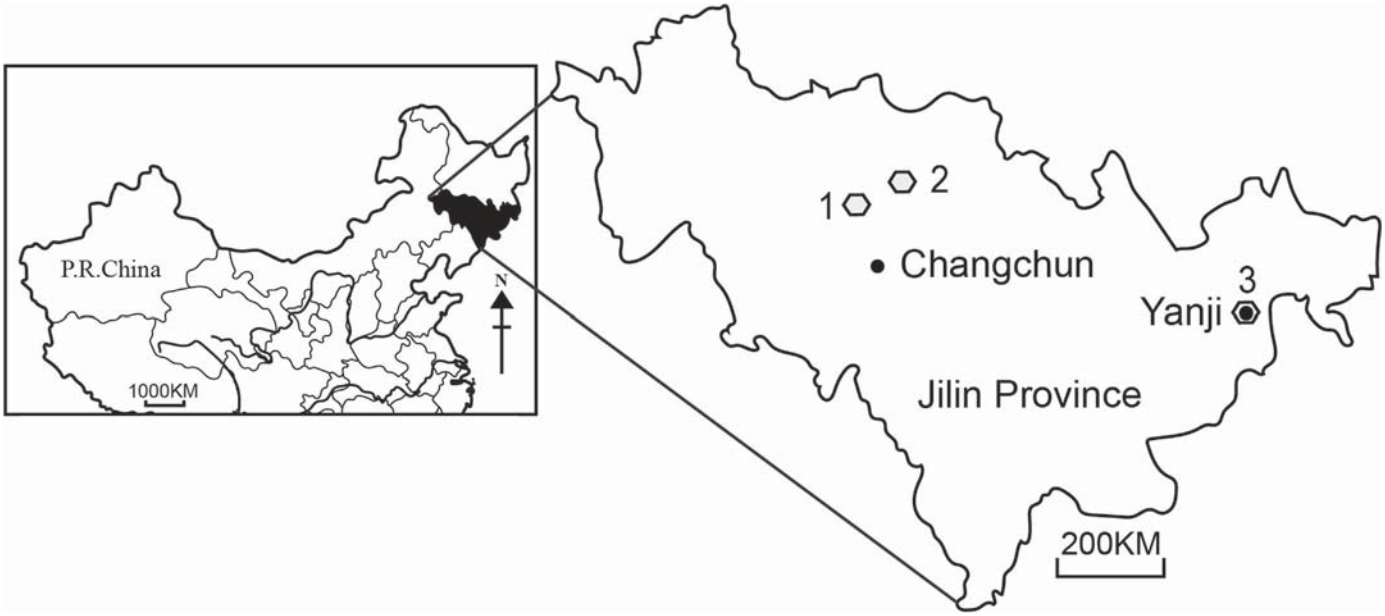

Fig. 1. A map showing localities across Jilin Province, China from which paralligatorid fossils have been recovered. 1. *Paralligator sungaricus* (Sun, 1958); 2. *Rugosuchus nonganensis* (Wu et al., 2001a); 3. *Yanjisuchus longshanensis* gen. et sp. nov., holotype (YJDM 00009).

Kuan (Chia-yu-kuan), Gansu were identified as *Paralligator* and *Chiayusuchus cingulatus* (Bohlin, 1953; Dong, 1974), respectively. However, due to their poor preservation, the aforementioned finds from Xinjiang were never used in any analysis, and although *Chiayusuchus cingulatus* was later considered a stomatosuchid (Carroll, 1988), it differs from teeth of that family (Sereno and Larsson, 2009).

In the present paper, we describe a new crocodyliform, *Y. longshanensis*, from the Longjing Formation of the mid-Cretaceous, which is the third fossil crocodyliform species known in Jilin Province. Numerous dinosaurian and testudine fossils were recovered together with the crocodyliform specimen from the formation in Yanji, representing the largest known dinosaur fauna in Jilin Province and also the eastern most dinosaur fauna found in China (Jin et al., 2018). The Longjing Formation may be correlative with the Quantou Formation of the Songliao Basin in Jilin Province, which yielded many well-preserved fossils of dinosaurs, mammals, and dinosaur eggs (Wang et al., 2006; Jin et al., 2009).

Paralligator was first introduced by Konzhukova in 1954 when she was describing *Paralligator gradilifrons* from the Upper Cretaceous Bayanshiree Formation in Shireegin Gashoon, Mongolia. *Paralligator sungaricus* was the first crocodyliform discovered in Jilin Province, and was collected from the Nenjiang Formation of Dehui County in the Song-Liao Plain. Recently, it has been considered as a *nomen dubium* (Turner, 2015). *Rugosuchus nonganensis* was the second crocodyliform reported from the province, also collected from the Nenjiang Formation but in Nong'an County, about 44 km southwest of Dehui. The Nenjiang Formation was originally assigned to the Lower Cretaceous, but was referred to the Upper Cretaceous by the most recent study, with an age ranging from 82.8 to 85.2 Ma (Yu et al., 2019), covering most of the Santonian to the early Campanian.

In this paper, we focus on the osteology, taxonomy and phylogenetic position of the new taxon, *Yanjisuchus longshanensis*. The discovery of the new crocodyliform not only enriches our knowledge of the distribution and evolution of neosuchians, especially the Paralligatoridae in northeastern China and Central Asia, but also provides new information to stimulate the study of the terrestrial biodiversity, paleoecology, and paleogeography of dinosaur faunae in Northeast Asia during the Cretaceous.

2. Geological settings

The Cretaceous strata in the Yanji Basin include, from bottom to top, the Tuntianying Fm., Changcai Fm., Toudao Fm., Tongfosi Fm., Dalazi Fm., and Longjing Fms. (Cui et al., 1994). The ages of the Dalazi and Longjing Formations have been controversial for years (Zhang, 1980; Zhang, 1986; Shi, 2008). Some studies considered the Longjing Formation to be Aptian (Matsukawa et al., 1995; Li et al., 2016), but other studies suggested it to be Cenomanian age (Shi, 2008; Jin et al., 2018) (Fig. 2). New ostracod data and radiometric dates for the underlying Dalazi Formation suggested an Albian–Cenomanian age for the Longjing Formation (Zhong et al., 2020).

The Longjing Formation crops out mainly on both sides of the Burhatong River valley and the surrounding hills in Yanji. It mainly consists of a set of red sediments of a fluvial phase (Zhang et al., 2015). The formation is divided into upper and lower units (Jin et al., 2018). The upper unit is a sand-shale section consisting of red, purple, and gray-green siltstones, with pebbled sandstones and thin layers of marlstones, partially sandwiching a thin layer of gypsum. The lower section is composed of grayish yellow, red pebbly sandstones and conglomerates, and purple-red, green-gray siltstones and conglomerates at the bottom (Yao et al., 1991; Jin et al., 2018).

3. Materials and methods

The specimen described in this paper is housed in the Yanji Dinosaur Museum (YJDM), Yanji City, China, under catelog number YJDM 00009. On July 13, 2017, the specimens were excavated from a locality with GPS Coordinates 41°52′10.0″N and 129°29′28.0″E, which is located on the south side of the Burhatong River, just right next to the current Yanji Dinosaur Museum.

The specimen were prepared with mechanical tools (air-scribes) and photographed using a Nikon D610 digital camera. The figures

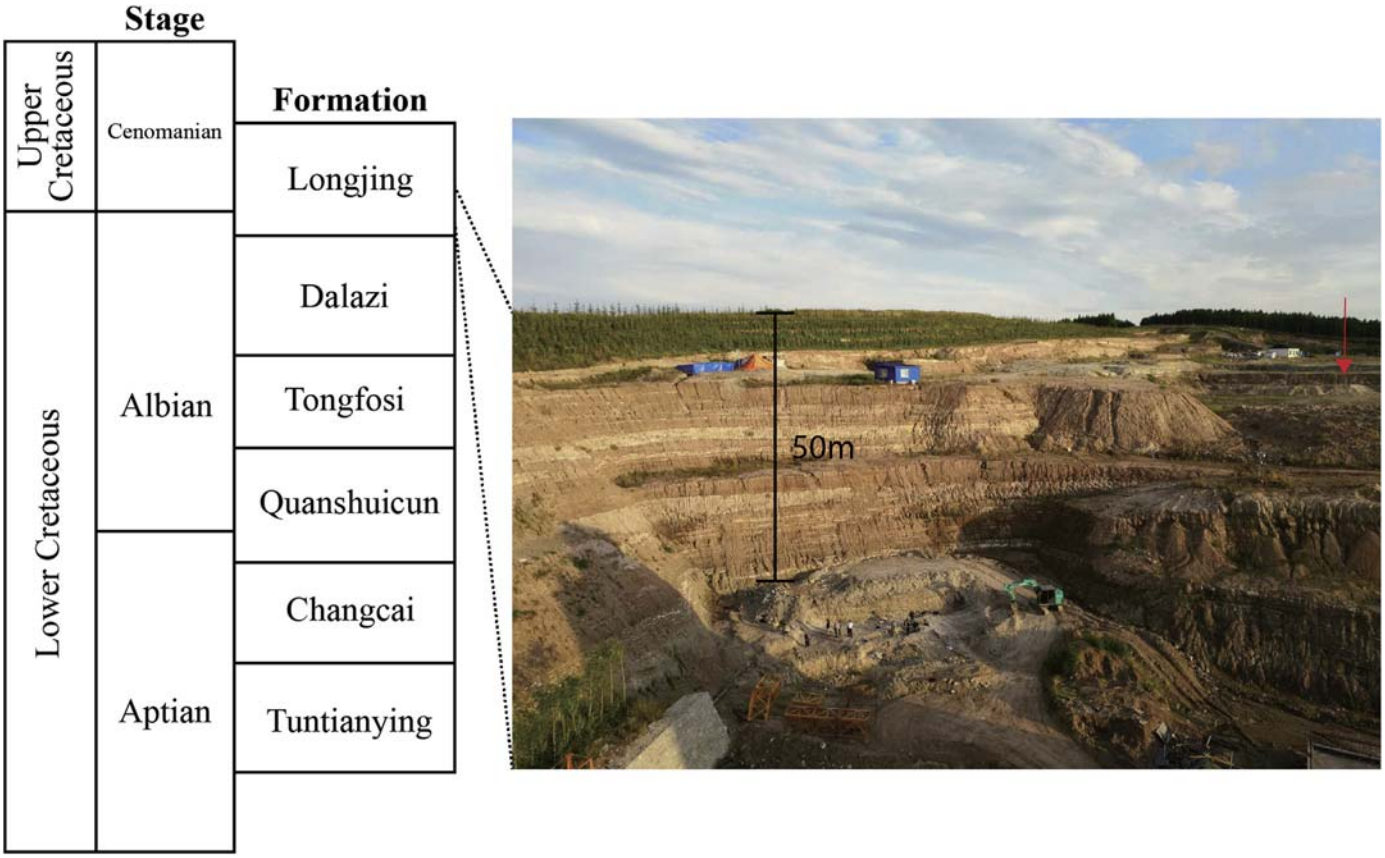

Fig. 2. Stratigraphic section of the Longjing formation in the Yanji Basin (derived from Zhong et al., 2020; Fig. 3).

were prepared using Adobe Photoshop CS6 and Adobe Illustrator CS6 software. Line drawings were made based on those photographs and checked against the original specimens. The leading author took all measurements of the specimen. Phylogenetic analyses were conducted using TNT v.1.5 (Goloboff and Catalano, 2016).

Institutional Abbreviations. IVPP, Institute of Vertebrate Paleontology and Paleoanthropology, Beijing, People's Republic of China; IGM, Mongolian Institute of Geology, Ulaan Baatar, Mongolia; YJDM, Yanji Dinosaur Museum, Yanji, Jilin Province, People's Republic of China.

Anatomical abbreviations. **acr**, acromion; **af**, articular facet, **ant,** anterior; **as**, articular surface; **asf**, sutural articular facet; **bcn**, blood channel; **boc**, basioccipital; **bos**, boss; **brk**, broken surface; **bsp**, basisphenoid; **cf**, caudofemoralis flange; **cp**, capitulum; **cdy**, condyle; **cfo**, coracoid foramen; **CrA**, Crest A; **CrB**, Crest B; **CrC**, Crest C; **ctr**, centrum; **cqp**, cranioquadrate passage; **dct**, distal concavity to tibia contact; **dia**, diastema; **dp**, depression; **dpp**, diapophysis; **edc**, endocast; **eoc**, exoccipital; **eop**, exoccipital peg; **epp**, endocast of paratympanic pneumatic cavities; **exf**, external facets; **fae**, foramen aërum; **facf**, facies articularis capitis fibulae; **faif**, facies articularis inferior fibulae; **faml**, facies articularis malleoli laterali; **fmg**, foramen magnum; **for**, foramen; **fr**, femorotibialis ridge; **fro**, frontal; **fsa**, fossae; **hpp**, hypapophysis; **hrt**, humeral radialis tubercle; **grv**, groove; **gs**, glenoid surface; **gt**, greater trochanter; **ica**, internal carotid artery; **icg**, intercondylar groove; **iob**, interorbital ridge; **ipr**, intertympanic pneumatic recess; **ISTR**, scar corresponding to the attachment of M. ischiotrochantericus; **it**, *iliofibularis* trochanter; **itf**, infratemporal fenestra; **jug**, jugal; **lac**, lacrimal; **lat**, lateral; **lc**, lateral condyle; **lhc**, lateral hemicondyle; **lic**, linea intermuscularis cranialis; **max**, maxillae; **mc**, medial condyle; **mdr**, medial ridge; **mec**, middle ear cavity; **med**, medial; **met**, medial eustachian tube; **mhc**, medial hemicondyle; **mpc**, medial proximal crest; **nas**, nasal; **nc**, neural canal; **ns**, neural spine; **ncs**, neural canal suture; **nvf**, neurovascular foramen; **obr**, orbital margin; **ocn**, occipital condyle; **ofg**, olfactory groove; **opr**, otoccipital pneumatic recess; **orb**, orbital; **ovl**, overlapped; **par**, parietal; **pas**, proximal articulation surface; **pd2**, preserved tooth 2; **pd3**, preserved tooth 3; **pd4**, preserved tooth 4; **PIFI1**, **PIFI2**, scar corresponding to the attachment of M. pubo-ischio-femoralis internus 1 or 2; **pob**, postorbital; **poc**, posterior concavity; **pof**, popliteal fossa; **pog**, preorbital groove; **pop**, paraoccipital process; **por**, preorbital ridge; **poz**, postzygapophysis; **ppp**, parapophysis; **ppr**, parietal pneumatic recess; **prf**, prefrontal; **prz**, prezygapophysis; **qdj**, quadratojugal; **qdr**, quadrate; **ras**, radiohumeral articular surface; **rid**, ridge; **sap**, single articular process; **sca**, scar; **sfe**, supratemporal fenestrae; **sfo**, supratemporal fossae; **sqm**, squamosal; **sut**, suture; **sym**, mandibular symphysis; **thr**, thin ridge; **tb**, tuberculum; **tp**, transverse process; **trs**, triangular shaped; **wse**, wedge-shaped elevation; **vmp**, ventromedial process; **xsg**, x-shaped groove; **4tr**, fourth trochanter.

4. Systematic paleontology

Crocodylomorpha Hay, 1930 *sensu* (Walker and Westoll, 1970)
Crocodyliformes Hay, 1930 *sensu* (Clark 1986)
Neosuchia Benton & Clark, 1988
Paralligatoridae Konzhukova, 1954

Yanjisuchus gen. nov.

Etymology. Generic name refers to Yanji City, where the fossil locality is situated, and *suchus*, the Greek word for the Egyptian crocodile deity Sobek.
Type species: ***Yanjisuchus longshanensis*** sp. nov.

Yanjisuchus longshanensis sp. nov.
(Figs. 3-15)
(urn:lsid:zoobank.org:act: C0F36066-D6AD-4FA7-A8C9-1DA81D424459)

Diagnosis. As for the type and only known species.
Etymology. Specific name refers to Longshan Hill, where the specimens were collected.
Diagnosis. (* denotes autapomorphies in the context of other paralligatorids). A medium-large crocodyliform diagnosed by the following combination of derived characters: wedge-shaped elevation on the anterior part of the frontal; interorbital ridge along the midline and a grooved, transversely oriented preorbital ridge; a weak ridge running anteroposteriorly on the lateral surface of the jugal; posterior process of the jugal elongate and forming the entire infratemporal bar; mandibular symphysis elongate and formed by the fused dentaries; diastema posterior to the fourth dentary tooth*; coracoid and the scapula almost equal in length; the proximal quarter of the fibula strongly curving posteriorly; medial keel developed on the posterodorsal halves of the osteoderms; and more than two rows of dorsal osteoderms.
Holotype. YJDM 00009, a partial skull lacking most of the skull table, maxilla, premaxilla, and mandible, and postcranial elements including isolated vertebrae, ribs, left scapula, right coracoid, right radius, left ulnare, right femur, right fibula, metatarsals, and some dorsal osteoderms.
Locality and horizon. A construction site between Baomei Mountain Villa Park and Longhedong, Yanji city, Jilin Province; the Albian–Cenomanian Longjing Formation (Zhong et al., 2020; Shen et al., 2021).

5. Description

5.1. Skull

The unpaired frontal is well preserved, but its orbital margins are slightly damaged due to weathering (Figs. 3A and 4). The main body of the bone is thick and heavily ornamented with deep, oval-shaped pits on the dorsal surface. The frontal forms most of the medial orbital margin. The interorbital region is narrow, forming the central portion of the frontal's hourglass-shaped outline. A 27 mm long ridge runs along the midline of the interorbital region and thickens anteriorly before connecting with the transversely oriented preorbital ridge. The latter slightly curves posterolaterally at its ends and disappears at the anteromedial margins of the orbit. The preorbital ridge is grooved along its length. The frontal is depressed between the interorbital ridge and the preorbital ridge where it forms a concavity, this could be due to diagenesis. A distinct wedge-shaped elevation forms the anterior margin of the frontal body and extends transversely to the prefrontal (Figs. 3A and 4B-C). A small part of the left prefrontal and left lacrimal are preserved in articulation with the frontal. The frontal broadens slightly towards the preorbital ridge anteriorly but strongly expands towards the supratemporal fossa to meet the postorbital posterolaterally, and then narrows to meet the parietal posteriorly. The frontal forms a large part of the margin of the supratemporal fenestra, and the anteromedial border of the supratemporal fossa. The margins of the orbits and the supratemporal fenestrae are formed by a raised rim. The bar between the orbit and the supratemporal fossa is 9.77 mm broad, with heavy ornamentation on the dorsal surface. Only a small part of the left squamosal is preserved, and it meets the postorbital anteriorly. Ventrally, the frontal bears a shallow trench, the olfactory groove (Fig. 4A). A small part of the parietal remains articulated with the frontal.

The posterior third of the left supratemporal fossa (including the fenestral portion) is missing, and only the anteromedial part of the right supratemporal fossa is preserved (Fig. 3A). The fossa appears oval in outline as indicated by the preserved part and is evidently smaller than the orbit. The long axis of the supratemporal fossa is oriented anterolaterally-posteromedially, whereas in *Shamosuchus djadochtaensis* (Pol et al., 2009), *Rugosuchus nonganensis* (Wu et al., 2001a), and *Bernissartia fagesii* (Buscalioni and Sanz, 1990) the axis is parallel to the midline. The right infratemporal fenestrae is well preserved and is much larger than the supratemporal fossa (Fig. 3B). It is triangular and posteriorly elongated in outline. The anterior border, the postorbital bar, is broken dorsally, recessed, and unornamented.

The anterolateral part of the left postorbital is preserved but most of the descending process of the bone, which contributes to the postorbital bar, is missing (Fig. 3A). Most of the right postorbital is damaged, but the descending process is complete albeit broken into two parts (Fig. 3B). The postorbital forms one-third of the anteromedial border of the supratemporal fossa and the anterolateral corner of the skull table, which is almost squared-off. The corner is rounded in the bernissartiid *Koumpiodontosuchus* (Sweetman et al., 2015: fig. 3A), and bears an anterolateral process in *Elosuchus* (Turner, 2015: figs. 3 and 5; Meunier and Larsson, 2017: fig.6A). The dorsal surface of the postorbital is ornamented with shallow pits. A boss-like structure also seen in *Shamosuchus djadochtaensis* (Turner, 2015: fig. 7C) is present on the anterolateral corner of the postorbital. There are two small foramina which are above the base of the postorbital bar (Fig. 4A-B). The base of the postorbital body is slightly constricted and it sends a short process to meet the quadratojugal at the dorsal apex of the infratemporal fenestra as in *Shamosuchus djadochtaensis* (Pol et al., 2009: fig. 10). Ventrally, the postorbital bar overlaps the ascending process of the jugal to form an interdigitating suture (Fig. 5). The postorbital bar slightly broadens at the suture and it is cylindrical and solid.

The right jugal is better preserved than the left one, but cracked and incomplete (Fig. 3B). The ectopterygoid contacts the medial side of the jugal at the ventral base of the postorbital bar. The posterior process of the jugal is very long and forms the entire infratemporal bar. The external surface of the jugal is heavily ornamented. Anteriorly, the preserved part of the jugal extends at least to the anterior border of the orbit, but the anterior end is missing. The anterior part of the jugal is roughly twice as broad as the posterior process. There is no trace of a ridge on the external surface of the jugal, although such a ridge is present in *Shamosuchus djadochtaensis, Paralligator* spp. and *Kansajsuchus extensus* (Turner, 2015; Kuzmin et al., 2018). The jugal portion of the postorbital bar is unornamented, like the descending process of the postorbital. The medial surface of the jugal bears a shallow depression ventral to the orbital border at the base of the postorbital bar, as in *Shamosuchus djadochtaensis* (Turner, 2015) and *Batrachominus pastosbonensis* (Montefeltro et al., 2013).

The right quadratojugal is better preserved than the left one, although the ascending process of the former is somewhat damaged along the posterior margin of the infratemporal fenestra (Fig. 3B). The external surface of the bone is ornamented but the ascending process is not. Its suture with the quadrate is nearly straight and its suture with the jugal is short and almost vertical. The anterior process, which contributes to the ventral border of the infratemporal fenestra in *Shamosuchus*, is very rudimentary and indeed, almost absent. Posteriorly, the quadratojugal overlaps the quadrate and extends ventrally to the quadrate condyles. The dorsal end of the ascending process meets the postorbital along the dorsal

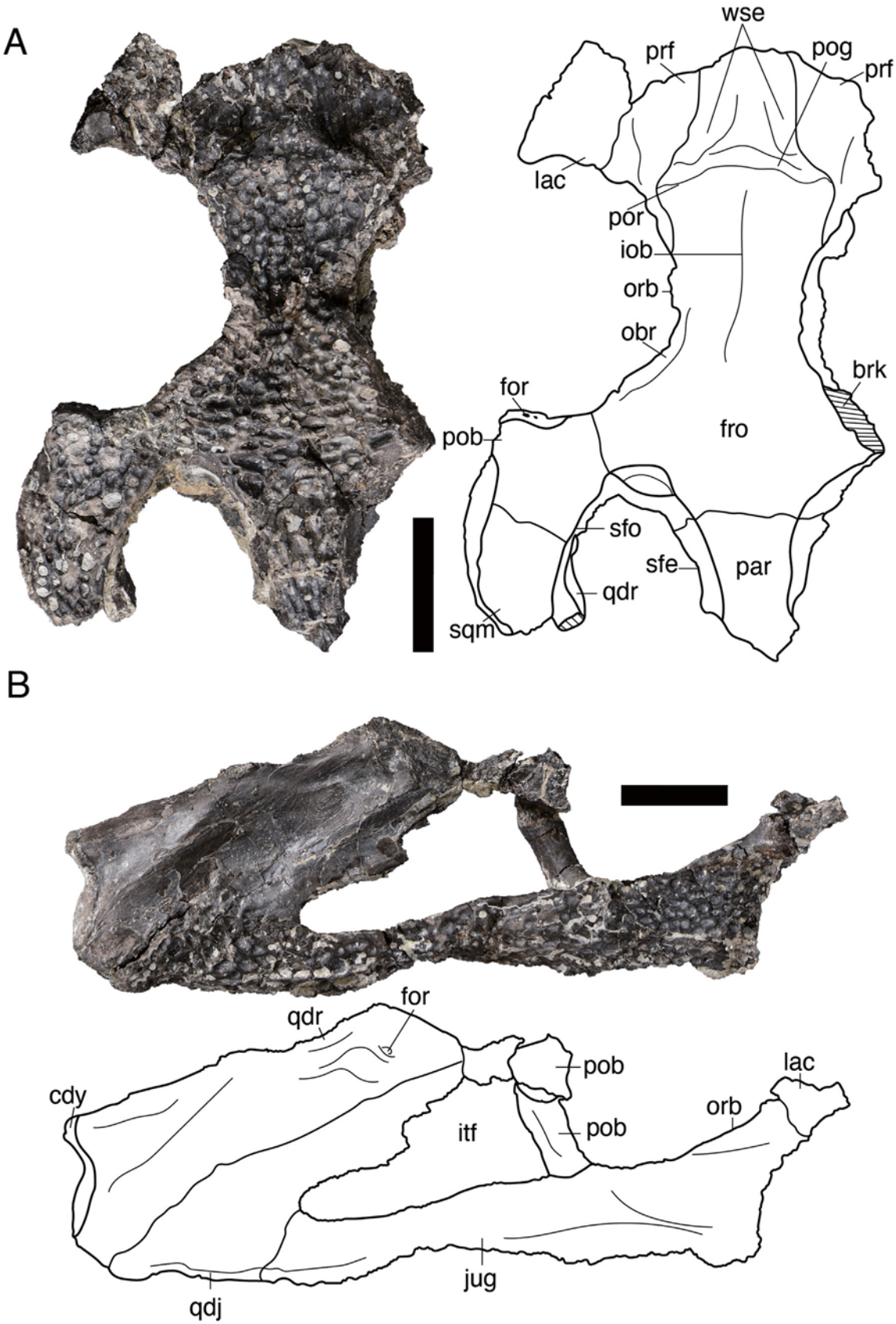

Fig. 3. Skull elements of *Yanjisuchus longshanensis* gen. et sp. nov., holotype (YJDM 00009). A, Posterior portion of the skull roof in dorsal view. B, Posterolateral portion of the skull in right lateral views. Scale bars each equal 2 cm.

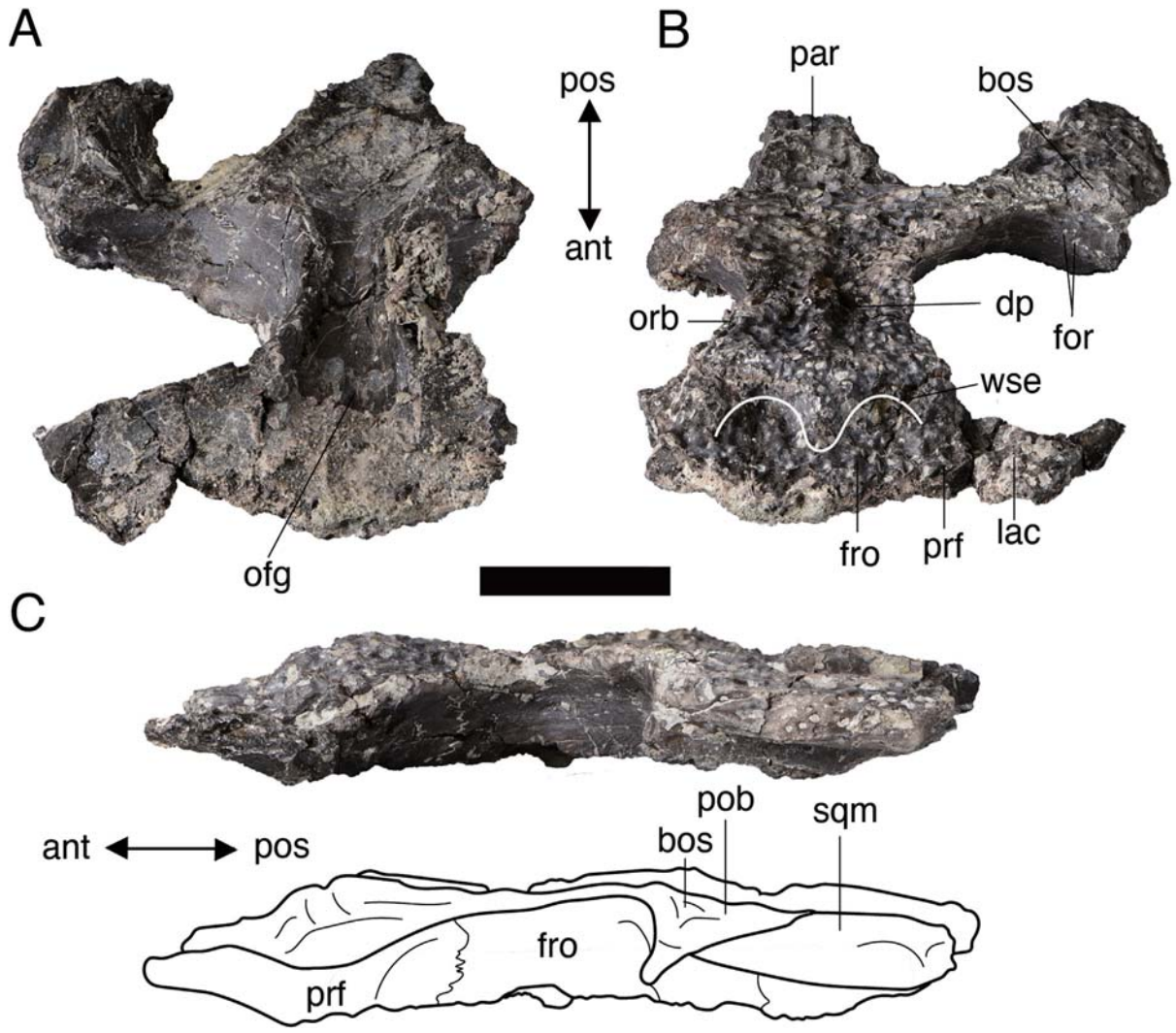

Fig. 4. Orbital region of *Yanjisuchus longshanensis* gen. et sp. nov., holotype (YJDM 00009) in oblique ventral (A), oblique dorsal (B), and left lateral (C) views. Scale bar = 2 cm.

border of the infratemporal fenestra, as mentioned earlier. As in *Shamosuchus* and most *Paralligator* species, there is no ridge along the dorsal section of the quadrate-quadratojugal contact. It is uncertain if a quadratojugal spine is present along the posterior border of the infratemporal fenestra, due to poor preservation.

The left quadrate is better preserved than the right, with the dorsal part missing on the latter (Figs. 6 and 7). The left quadrate is still articulated with the braincase although the latter is incomplete. The dorsal part of the left quadrate reaches the lateral surface of the braincase anteromedially and meets the exoccipital and the ascending process of the quadratojugal posteromedially. The cranioquadrate passage is visible, but whether the passage is open or closed is uncertain due to the absence of the squamosal. Ventrally, the quadrate condyle is deeply divided into a large lateral hemicondyle and a small medial hemicondyle. A foramen aërum is present and located far from the medial margin of the bone, dorsomedial to the medial hemicondyle. The lateral hemicondyle projects horizontally and the medial hemicondyle projects ventrally. On the ventral surface, Crest A and Crest B (Iordansky, 1973) are evident. Crest A runs down from the posteroventral margin of the supratemporal fenestra and meets closely to Crest B at the anteromedial part of the quadrate. Crest C (Iordansky, 1973) is short and weakly developed, running across the ventral surface of the main body close to the medial margin dorsal to the medial hemicondyle. Posterior to the juncture of Crest A and Crest B is a deep fossa. Other morphological features of the quadrate cannot be evaluated due to damage. The pterygoid is missing.

The basisphenoid is preserved, but the parabasisphenoid rostrum is missing (Fig. 6B and C), and the bone is exposed only as a V shaped outline visible in ventral view. It forms the anterior borders of the foramina of the median Eustachian tubes. Poor preservation obscures the sutures of the basisphenoid with the laterosphenoid and basioccipital, although a small part of the laterosphenoid is preserved on the left side of the braincase. The laterosphenoid contacts the quadrate posteriorly and forms the anterior part of the margin of the supratemporal fenestra.

The left otoccipital is better preserved than the right. The otoccipital is formed by the fusion of the opisthotic and the exoccipital. The paraoccipital process projects laterally and terminates in a prominent boss beyond the cranioquadrate opening (Fig. 6B and C). The foramen magnum is dorsoventrally narrow due to dorsoventral compression during preservation. Peg-like processes of the left and right otoccipitals meet dorsal to the foramen magnum, separating the supraoccipital from the foramen magnum. The

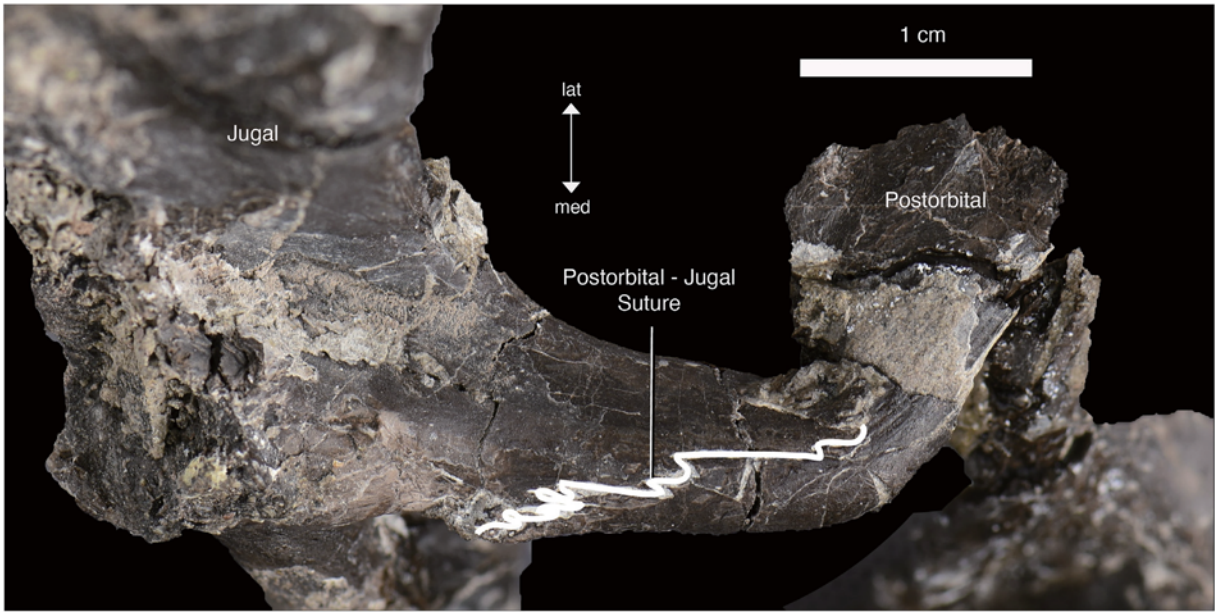

Fig. 5. Postorbital bar of *Yanjisuchus longshanensis* gen. et sp. nov., holotype (YJDM 00009) in posteromedial view.

sutures of the otoccipitals with the basioccipital are clear, running ventrolaterally. The sutures of the otoccipital with the quadrates anteriorly and the supraoccipital dorsally are preserved. The ventrolateral contact of the otoccipital with quadrate is broad. Only the left carotid foramen is visible, located entirely in the exoccipital part of the otoccipital. The supraoccipital is missing.

The basioccipital is nearly complete (Fig. 6B and C). The occipital condyle is oval and transversely broad, and forms the ventral border of the foramen magnum. Dorsolaterally, the basioccipital-exoccipital suture is clear. The ventral wing of the basioccipital is fan-like or 'W'-shaped and nearly vertical in orientation. Ventrally and ventrolaterally, the wing contacts the basisphenoid and forms the posterior border of the medial opening of the Eustachian tube; presumably also bordered the foramen of the lateral Eustachian tube on both sides although the relevant areas have been damaged (Fig. 6C).

A segment of the right dentary is preserved (Fig. 8), and is 53 mm long and 23 mm wide in dorsal view. In the anterior half of the segment, the mandibular symphysis is clearly visible in dorsal and ventral views (Fig. 8A and B). The U-shaped posterior end of the symphysis indicates that the midline of the symphysis is preserved, but it does not show any trace of a suture, which means that the two dentaries might have fused as in the basal crocodyliform, *Platyognathus hsui* (Wu and Sues, 1996b), or it could be caused by poor preservation. In ventral view, a shallow triangular depression is present posteriorly along the midline of the symphysis, with a sharp apex pointing anteriorly. The slightly expanded anterolateral margin (curving outwards) and concave dorsal surface of the dentary segment indicate that it most probably represents the portion of the bone situated just posterior to the large fourth dentary tooth. This suggests that the symphysis was long and extended posteriorly well beyond dentary tooth 4 in life. The dorsal and dorsolateral surfaces of the dentary segment are smooth, while the ventral surface is ornamented with pits and short ridges. The medial surface of the dentary is slightly concave and bears a shallow depression just posterior to the symphysis. In dorsal view, there are two empty alveoli and a partially damaged tooth preserved in the posterior half of the segment. As indicated by the alveoli, the three teeth become larger posteriorly; the first preserved alveolus is smallest and the second is evidently larger than the first but only reaches half the diameter of the preserved tooth crown. The anterior half of the dentary segment does not bear any alveoli or teeth, indicating an unusually broad diastema posterior to the fourth dentary tooth. The dorsal surface of the dentary segment evidently rises up just posterior to the diastema, leading to an increase in the height of the dentary posteriorly as in *Araripesuchus, Shamosuchus* and other neosuchians (Ortega et al., 2000; Pol and Apesteguía, 2005; Turner, 2015). A large neurovascular foramen (Pol and Apesteguía, 2005) perforates this lateral surface. Posterior to the symphysis, no suture is visible on both the dorsal and ventral surfaces, indicating that the splenial was far from the mandibular symphysis anteriorly.

The aforementioned dentary tooth is the only one preserved in the jaws. Its apical end is missing. An isolated globidont tooth was collected in association with the specimens (Fig. 9). It is mushroom-like in outline, with a short, striated crown that bears striations and a slightly constricted base. A depression on the posterior surface of the crown might represent a wear facet (Fig. 9D). The aforementioned features indicate that this tooth most probably belongs to the posterior part of the dentition.

5.2. Axial skeleton

The four preserved vertebrae include one cervical, two dorsals, and one caudal (Fig. 10). They are all incomplete and amphicoelous. The preserved cervical (Fig. 10A-D) has a prominent hypapophysis at the anterior margin of the centrum and projects posteroventrally. The subtriangular parapophysis is adjacent to the anterior margin of the centrum, and is not far from the hypapophysis in ventral view. The centrum is 18.5 mm long. Both lateral surfaces of the centrum are deeply concave, with a foramen-like pit in the center rather than shallow grooves as in *Shamosuchus djadochtaensis* (specimen IGM 100/1195 in Turner, 2015). The diameter of the neural canal is similar in outline and diameter to the cup-like articular surfaces of the centrum. The diapophyses, whose ends are broken away, are located on the anterior half of the centrum as in *C. americanus* and *A. sinensis*. The diapophyses project ventrolaterally and slightly posteriorly. The suture of the neural arch with the

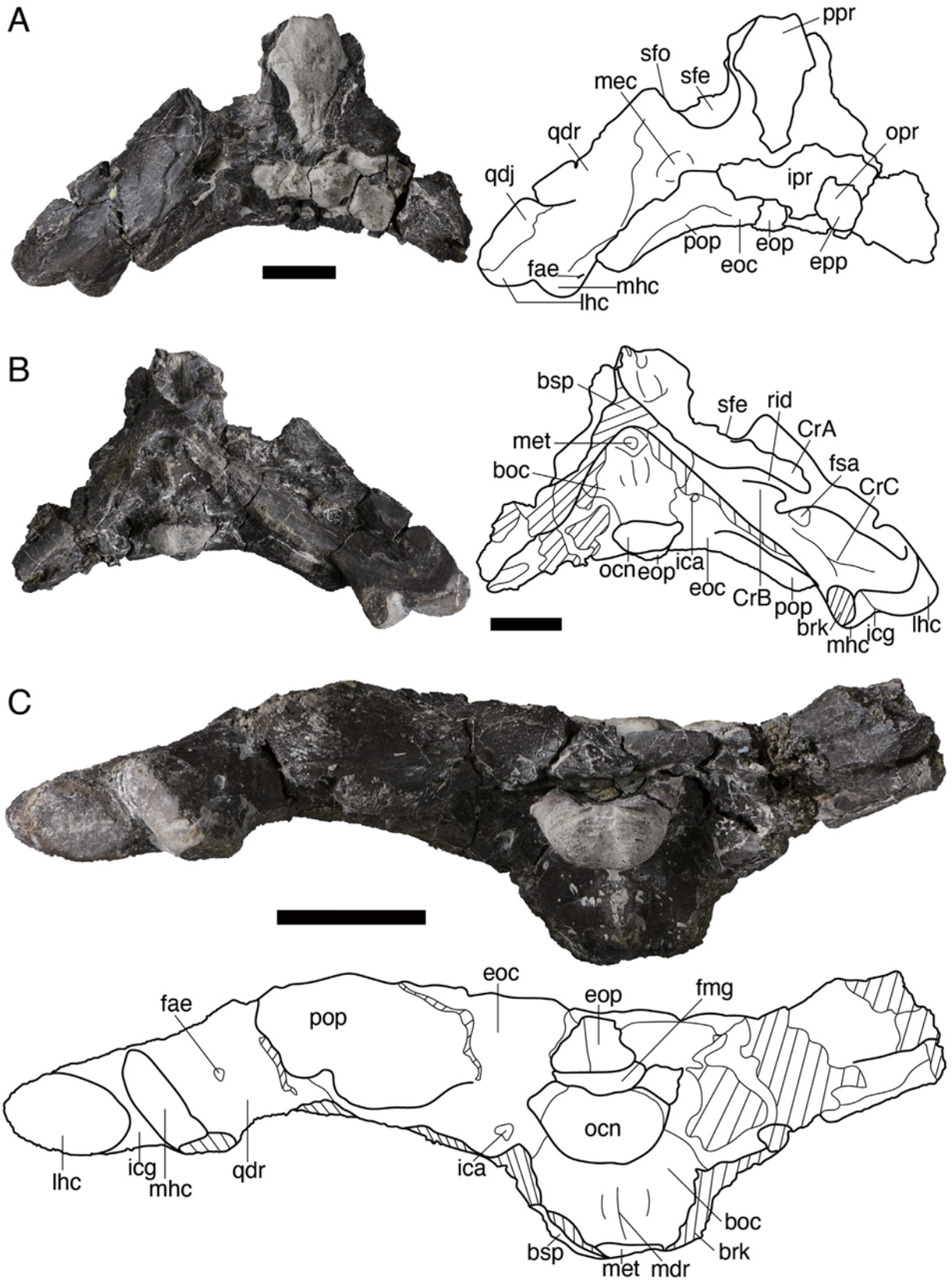

Fig. 6. Braincase and quadrate of *Yanjisuchus longshanensis* gen. et sp. nov., holotype (YJDM 00009) in dorsal (A), ventral (B), and posterior (C) views. Scale bars each equal 2 cm.

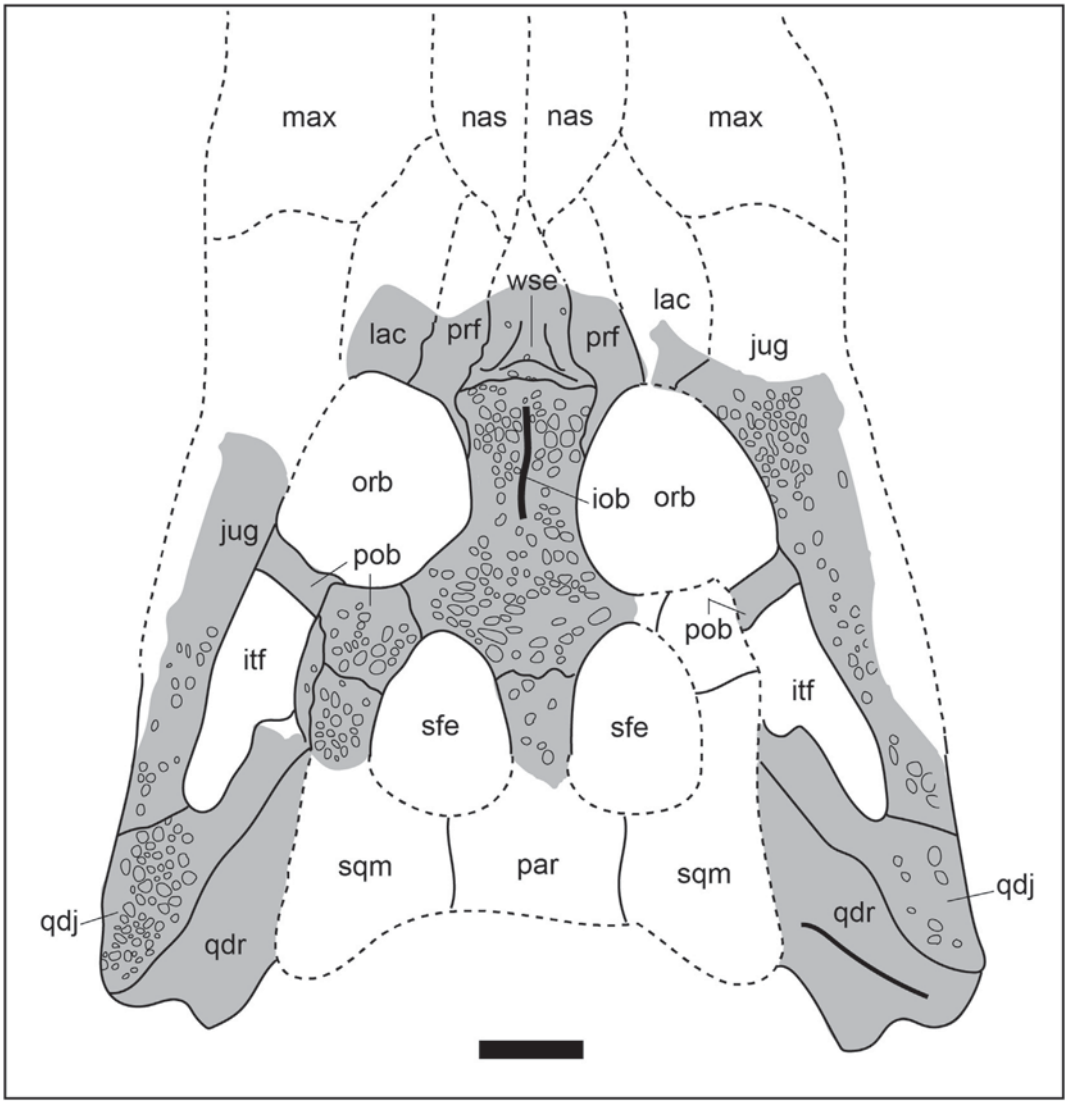

Fig. 7. Reconstruction of the preserved skull elements of *Yanjisuchus longshanensis* gen.et sp. nov., holotype (YJDM 00009) in dorsal view. Solid lines and areas in gray indicate the preserved parts. Scale bar = 2 cm.

centrum is fused, which suggests that the specimen represents an adult. The right prezygapophysis is complete, projecting anterodorsally, slightly beyond the anterior limit of the vertebral centrum; this is in contrast with the *Pissarrachampsa sera*, in which the prezygapophysis does not extend past the anterior limit (Godoy et al., 2016). The lateral surface of the prezygapophysis bulges laterally and the medial surface is concave. A groove is present between the prezygapophysis and the base of the neural spine, but the rest of the spine is not preserved. The suprapostzygapophyseal lamina (*sensu* Pol, 2005) extends from the dorsal edge of the postzygapophysis to connect with the posterior edge of the neural spine. This is similar to the condition seen in the third cervical vertebra of *Notosuchus terrestris*, but differs from the condition in the posterior-most cervicals of the Crocodylia, in which the lamina comes from the posterolateral edge of the neural spine (Frey, 1988; Pol, 2005). The right postzygapophysis, medial lamina and *incisura vertebralis caudalis* are missing. On the left lateral surface of the neural arch, a shallow fossa is present at the junction between the diapophysis and the pre- and postzygapophyseal laminae.

The centra of the two dorsal vertebrae differ in shape, one being cylindrical and the other spool-shaped. The neural spine is missing in the first dorsal vertebra and the parapophysis is fused with the diapophysis to form an undifferentiated transverse process (Fig. 10E-H). The left transverse process is damaged but the right transverse process is almost complete, with the distal end slightly weathered. The transverse process is thin, flat and rugose with the tuberculum and the capitulum facets are not distinctly separated, and must have articulated with a single-headed rib as in the extant *A. sinensis*. The neural canal is very small. Both prezygapophyses are broken away. The left postzygapophysis is almost complete, but the right postzygapophysis is not, due to preservation conditions. The articular surfaces of the postzygapophyses are nearly horizontal, almost parallel to the transverse process, as in *Notosuchus terrestris* (Pol, 2005) and the Crocodylia (Frey, 1988). Posteriorly, a groove is present between the postzygapophysis and the neural spine. The diapophysis is higher than the parapophysis. The centrum is cylindrical in shape, with a maximum length of 24.5 mm. The suture between the neural arch and centrum is not visible, as in the aforementioned cervical vertebra.

The second dorsal vertebra is partially preserved. The maximum length of the centrum is 25.3 mm (Fig. 10I-L). The suture between the neural arch and centrum is visible on both sides of the vertebra;

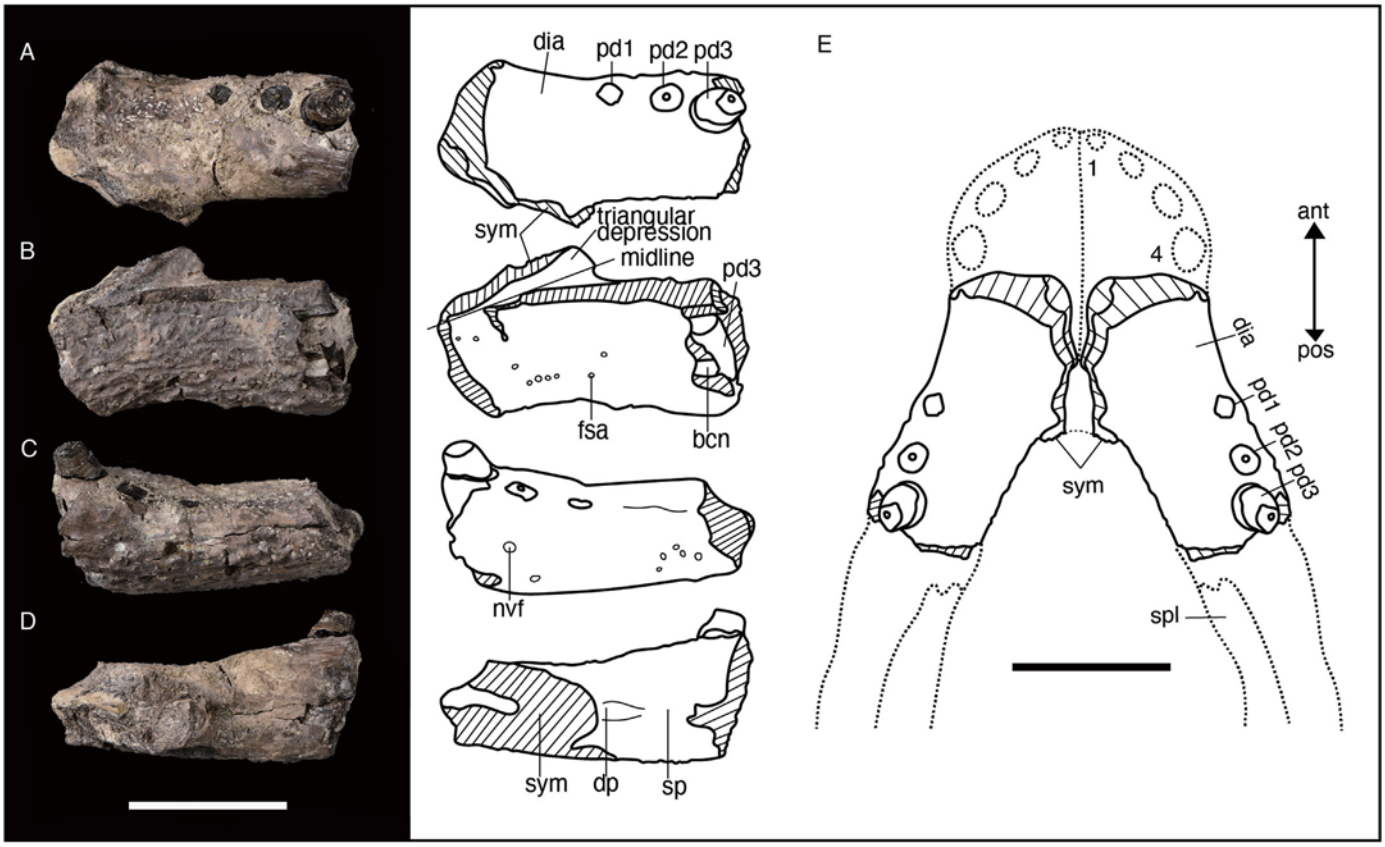

Fig. 8. Preserved part of the right dentary of *Yanjisuchus longshanensis* gen. et sp. nov., holotype (YJDM 00009) in dorsal (A), ventral (B), lateral (C), and medial (D) views and reconstruction of the symphysis of the lower jaw (E). Oblique lines indicate areas of broken surface. Scale bar = 3 cm.

Fig. 9. An isolated molariform tooth of *Yanjisuchus longshanensis* gen. et sp. nov., holotype (YJDM 00009) in labial (A), lingual (B), anterior (C), posterior (D), apical (E), and basal (F) views. Scale bar = 1 cm.

this is in sharp contrast to the fused condition in the previously described vertebra. The neural canal is much smaller than the centrum in diameter. The slightly broken prezygapophyses are anterodorsally positioned, and each bears a smooth facet facing more dorsally than medially. The right transverse process is nearly complete. It is thin and flat, but much shorter than that of the another dorsal vertebrae. The left postzygapophysis is incomplete, but like the prezygapophyses, does not protrude beyond the articular surface of the centrum. The neural spine is posteriorly thick and anteriorly thin. The dorsal surface of the spine expands into a leave-shaped table. Medial laminae (*sensu* Pol, 2005) are evidently present between the suprapostzygapophyseal laminae.

The preserved caudal vertebra is well preserved. The transverse processes are nearly complete, but both have slightly damaged ends (Fig. 10M–P). The neural spine is incomplete, with its anterodorsal part missing. Both prezygapophyses are broken away, leaving a small portion of their bases. Both postzygapophyses are present, with their posterior edges damaged. The centrum is maximally 28.7 mm long. It is transversely compressed, in contrast to the cylindrical centrum of the Crocodylia but similar to *Baurusuchus* (Nascimento and Zaher, 2010). In ventral view, the articular facets for the chevron are clearly evidently. The neurocentral suture is visible.

A preserved rib is considered to be an anterior dorsal rib with its distal section missing. It may be the first or second dorsal rib of the

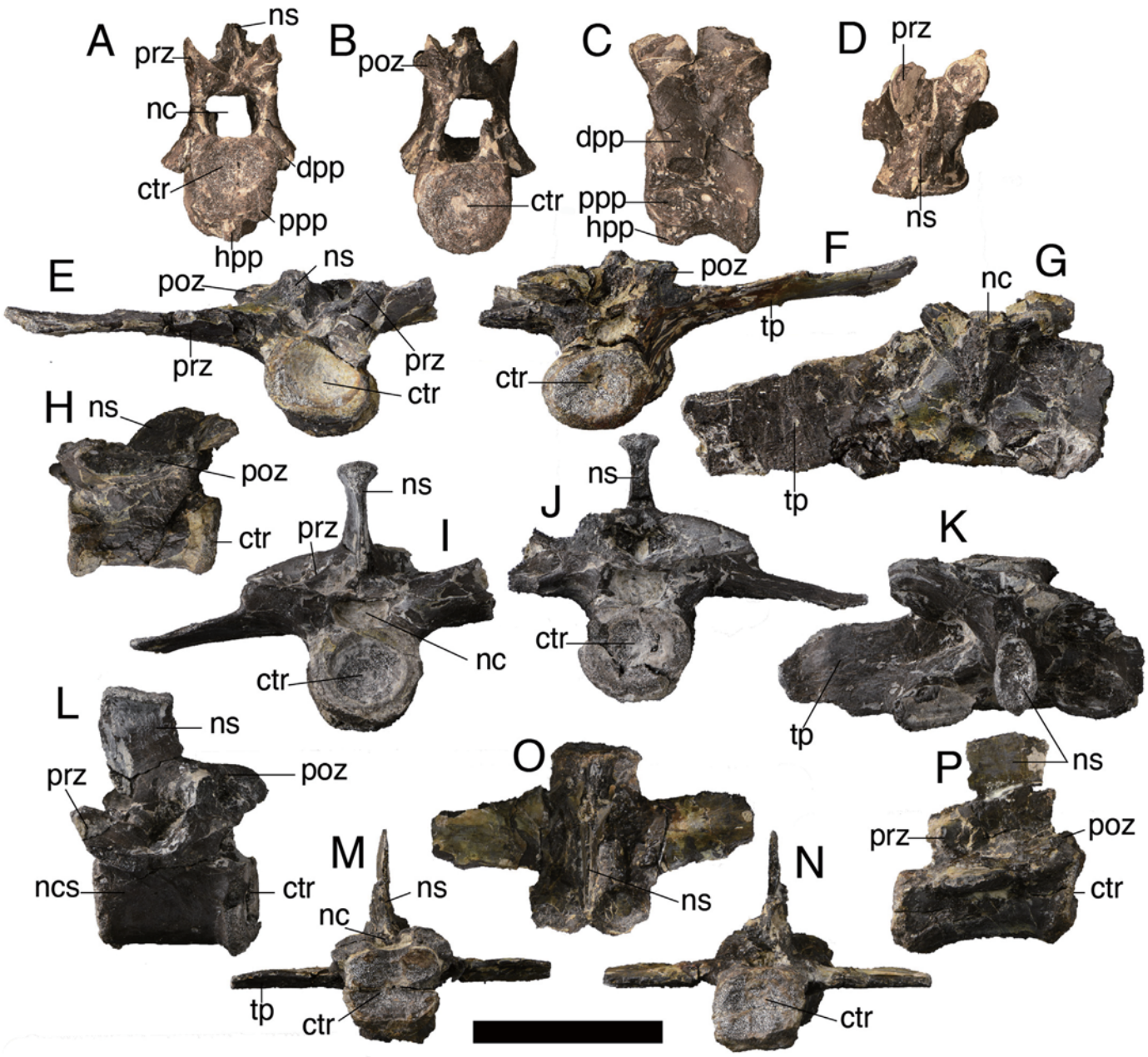

Fig. 10. Vertebrae of *Yanjisuchus longshanensis* gen. et sp. nov., holotype (YJDM 00009). A cervical vertebra in anterior (A), posterior (B), left lateral (C), and dorsal (D) views. E-H, A dorsal vertebrae in anterior (E), posterior (F), dorsal (G), and left lateral (H) views. Another dorsal vertebra in anterior (I), posterior (J), dorsal (K), and left lateral (L) views. A caudal vertebra in anterior (M), posterior (N), left lateral (O), and dorsal (P) views. Scale bar = 3 cm.

left side given the presence of an elongated tuberculum and capitulum (Fig. 11). It is exposed in medial view, with a concave surface. Its shaft is evidently curved anteroposteriorly, and becomes thicker distally. The tuberculum is somewhat shorter and thicker than the capitulum. The total length of the rib cannot be determined.

5.3. Appendicular skeleton

The preserved left scapula is not complete, the distal part of the dorsal blade being damaged (Fig. 12A and B). The preserved part indicates that the anterior margin of the blade broadens anterodorsally but not posterodorsally, and that the blade is thinner than the proximal region of the scapula. The posteroventral edge is thicker than the anteroventral edge. The lateral surface is flat but rugose, with scars marking the insertions of *m. teres major* and *m. deltoideus scapularis* (Cong et al., 1998; Meers, 2003). The surface of the blade is damaged, but is slightly concave, with a depression and grooves associate with attachment of muscles such as *m. subscapularis*. The anterior margin of the constricted area that separates the dorsal blade from the proximal part is partially damaged, but the area is clearly dorsoventrally short and relatively anteroposteriorly wide. The posterior area of the scapular blade between the insertion of *m. triceps longus caudalis* and the mainly laterally positioned tubercle for the insertion of *m. triceps longus lateralis* is rather flat. The surface of the tubercle is deeply concave.

In lateral view, the nearly complete acromion forms a long and prominent crest (37 mm in length). The surface posteroventral to the acromion and anterior to the tubercle is deeply concave. The articular surface of the glenoid is flat, facing mainly ventrally. The articular facet on the scapular for the coracoid is 39 mm wide and strongly uneven with rugosity.

The right coracoid is complete (Fig. 12C and D). The proximolateral surface is flat. The articular (dorsal) border with the scapula is about 33 mm wide and the ventral end reaches 29 mm in width. The similarities between these measurements is in sharp contrast to the condition in *Pachycheilosuchus trinquei*, in which the ventral end of the coracoid is less than half the width of the articular border (Rogers, 2003). The flat midshaft is 12 mm in width, in sharp contrast to the rod-like midshaft of *Chimaerasuchus paradoxus* (Wu and Sues, 1996a). The lateral midshaft surface of the coracoid is convex while the medial surface is strongly concave. The coracoid foramen is relatively large and located in the center of the dorsal part of the bone. A groove is present distal to the foramen laterally, and runs posteriorly to reach the bone margin distal to the glenoid. The glenoid surface is flat, and faces dorsolaterally. The posterior margin of the shaft is much more concave than the anterior margin. The distal end is strongly convex. In medial view, a scar on the anterodistal surface may have served for the attachment of *m. costocoracoideus superficialis* (Meers, 2003).

The right radius is preserved, with minor damage at both the proximal and distal ends and to the shaft (Fig. 12 E and F). In general, it is slender and morphologically similar to that of *Pachycheilosuchus trinquei* (Rogers, 2003). It is maximally 74 mm long and 7.3 mm wide. The proximal end is slightly more expanded than the distal end, a common character in Crocodyliformes (Pol, 2005). The radiohumeral articular facet is concave and its posterior part is broader than its anterior part. The proximal and distal portions of the bone are both compressed, with a triangular cross-section. Anteromedially, striations and a tubercle are present near the proximal end of the bone, and may have served for the attachment of *m. humeroradialis* (Meers, 2003). The shaft is almost cylindrical in outline, with a very distinct ridge for the insertion of *m. pronator teres*. The distolateral surface is smooth, whereas the posterior surface is rugose. In medial view, a strong fossa is present just dorsal to the distal end. The distal articular facet is convex, to fit into the proximal concavity of the radiale.

The preserved left ulnare is incomplete at both ends, so the exact length of the bone is unknown (Fig. 12G and H). The minimal width is around 5.5 mm. A triangular process on the medial side of the proximal end would have contacted the radiale. The ulnare has a thick cylindrical shaft.

The preserved right femur is complete. It has a gently sigmoidal curve, but it is relatively straight in anterior and posterior views (Fig. 13). It is 137 mm long in total and its midshaft is minimally 12 mm wide. Its midshaft is not entirely cylindrical, rather it is ovoidal and slightly flattened on lateral and medial views. The proximal and distal ends differ little in width, being about 32 mm or 33 mm wide, respectively. The proximal articular surface is convex. The femur and other limb bones are often missing in fossil crocodyliforms, which limits comparisons with other taxa. The femur is similar to those of *Kansajsuchus extensus* (Kuzmin et al., 2018: fig. 14) and early alligatoroids such as *Stangerochampsa mccabei* (Wu at al., 1996b: figs. 4-6 in Plate 3). In these taxa, the proximal portion dorsal to the anterior curvature is relatively long and the curvature is relatively shallow. In contrast, the proximal portion is short and

Fig. 11. An anterior dorsal rib of *Yanjisuchus longshanensis* gen. et sp. nov., holotype (YJDM 00009) in medial view. Scale bar = 3 cm.

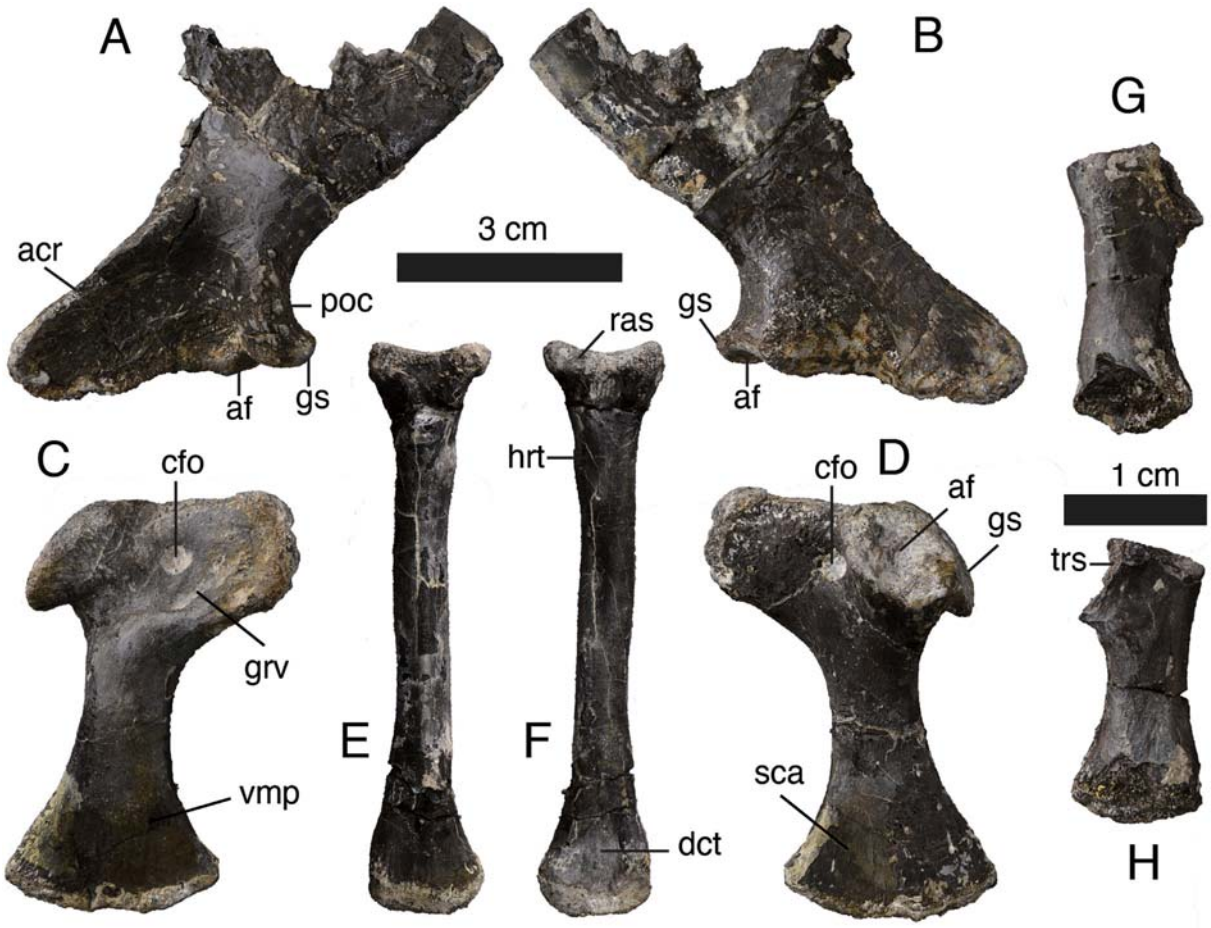

Fig. 12. Pectoral and forelimb elements of *Yanjisuchus longshanensis* gen. et sp. nov., holotype (YJDM 00009). Left scapula in lateral (A) and medial (B) views. Right coracoid in lateral (C) and medial (D) views. Right radius in lateral (E) and medial (F) views. Left ulnare in anterior (G) and posterior (H) views. Scale bars = 3 cm for A-F and 1 cm for G-H.

the curvature is deep in basal neosuchians such as *Sunosuchus junggarensis* (Wu et al., 1996a: fig. 15D-F) or basal crocodylians such as *Borealosuchus threeensis* (Brochu et al., 2012: fig. 3K and L). The greater trochanter is located posterodorsally. A strap-like rough surface from the trochanter extends distally but stops before it meets the fourth trochanter, and this rough surface presumably served for the insertion of *m. puboischiofemoralis externus* as in extant alligators (Cong et al., 1998: fig. 117; Hutchinson, 2001: fig. 1). With regard to features related to attachments of pelvic muscles, the femur shows a very similar condition to that seen in extant alligators (Romer, 1923; Cong et al., 1998; Hutchinson, 2001). A longitudinal ridge on the posteromedial surface, the longitudinal 'femorotibialis' ridge (*sensu* Godoy et al., 2016), is evident, which has been taken as an indication of adulthood for some fossil taxa (Godoy et al., 2016). The distal condyles are well developed. The intercondylar fossa is shallow as in *S. djadochtaensis* (Pol et al., 2009) and *Kansajsuchus extensus* (Kuzmin et al., 2018). The lateral condyle is much larger than the medial condyle. Both anterior and posterior surfaces of the distal femur bear both the medial and lateral supracondylar ridges, while the popliteal fossa is noticeable on the posterior surface, between both of the supracondylar ridges. Anterodistally, apparent minor scars in the form of shallow grooves or furrows are present on the articular surface for the fibula, but they may have been made by erosion.

The right fibula is complete, long and slender (Fig. 14A and B). It is similar to the fibulae of crocodylians (Mook, 1921). The fibula is maximally 104 mm long, and is shorter in comparison to the femur (about 76% the length of the latter bone) than in the neosuchian *Terminonaris robusta* (about 88%, Wu et al., 2001b: fig. 7) or extant alligators such as *A. sinensis* (about 80%, Cong et al., 1998). The proximal quarter of the fibula proximal to the *iliofibularis* trochanter curves more strongly posteriorly than in the aforementioned taxa and *S. junggarensis* (Wu et al., 1996a: fig. 15G), which is unique among neosuchians in which the bone is known. The triangular articular facet for the tibia is smooth, but striations representing muscle scars are present distal to the facet. The proximal end is more expanded (12.8 mm wide) than the distal end (10.8 mm wide). The shaft of the bone distal to the *iliofibularis* trochanter is straight and about 7 mm wide. The proximal and distal ends are flattened, while the shaft is oval in cross-section. In lateral view, the *iliofibularis* trochanter is about 6 mm long. A shallow depression is present proximal to the trochanter. On both the lateral and medial surfaces of the distal part of the bone is a triangular depression within which there are distinct grooves. These structures were probably due to postmortem damage, given the presence of cracks around the depressions. The articular facet for the calcaneum and, probably, astragalus is rectangular, which differs from a triangular facet for those bones in the extant alligator *A. sinensis* (Cong et al., 1998: fig. 89D).

Right metatarsal II is completely preserved (Fig. 14C and D). It is maximally 60.82 mm long and its shaft is 6.95 mm wide. The proximal ends are flat and a shallow depression is present on the

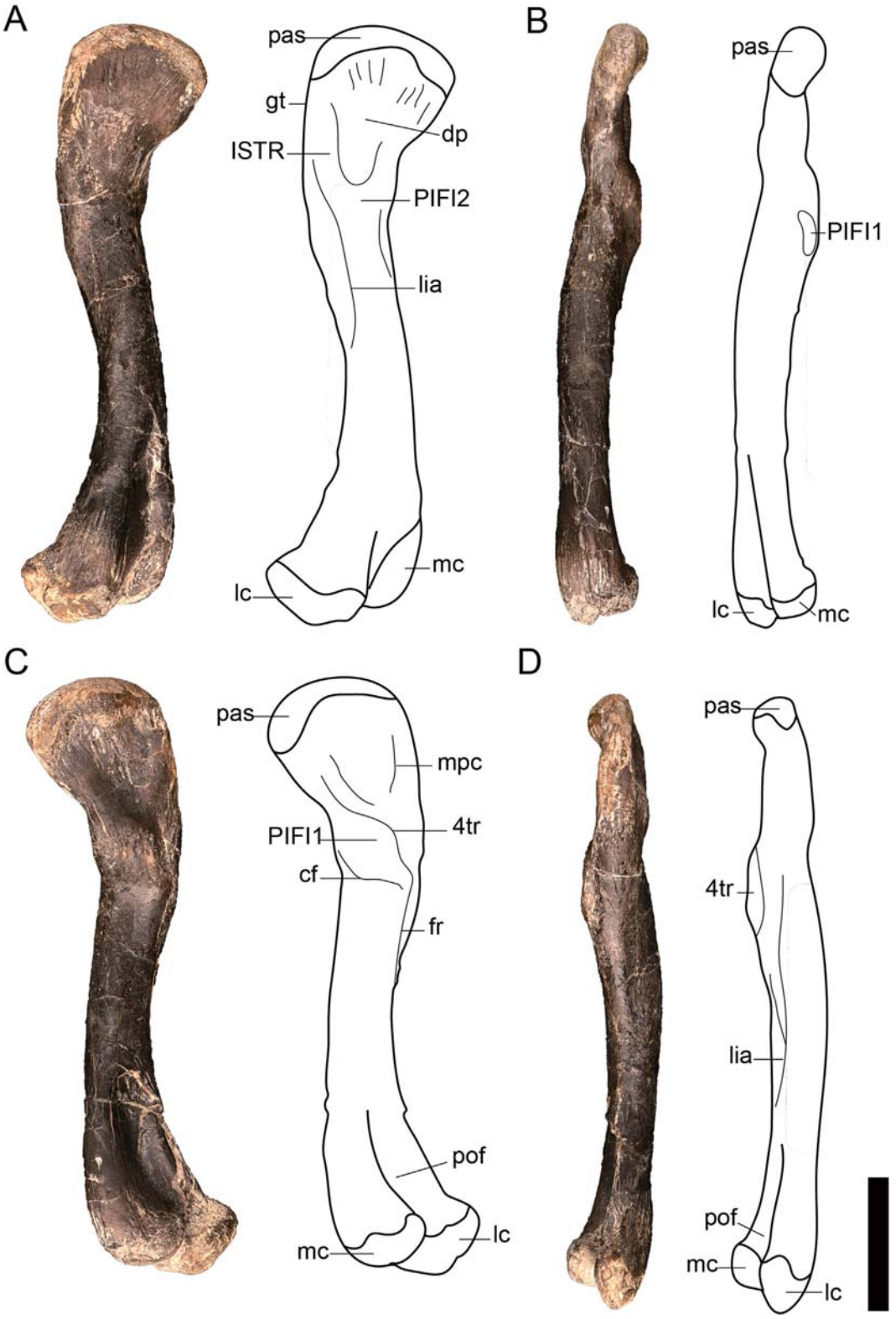

Fig. 13. Right femur of *Yanjisuchus longshanensis* gen. et sp. nov., holotype (YJDM 00009). in lateral (A), anterior (B), medial (C), and posterior (D) views. Scale bar = 3 cm.

dorsal surface. The depression appears to receive the overlap of metatarsal I and is not present on the first metatarsal in typical crocodyliforms (Nascimento and Zaher, 2010). The proximal head expands ventrally, and the rugosity of the articular surface for a distal tarsal was obviously caused by erosion. The metatarsal shaft is convex dorsally and concave ventrally, with an elliptical cross

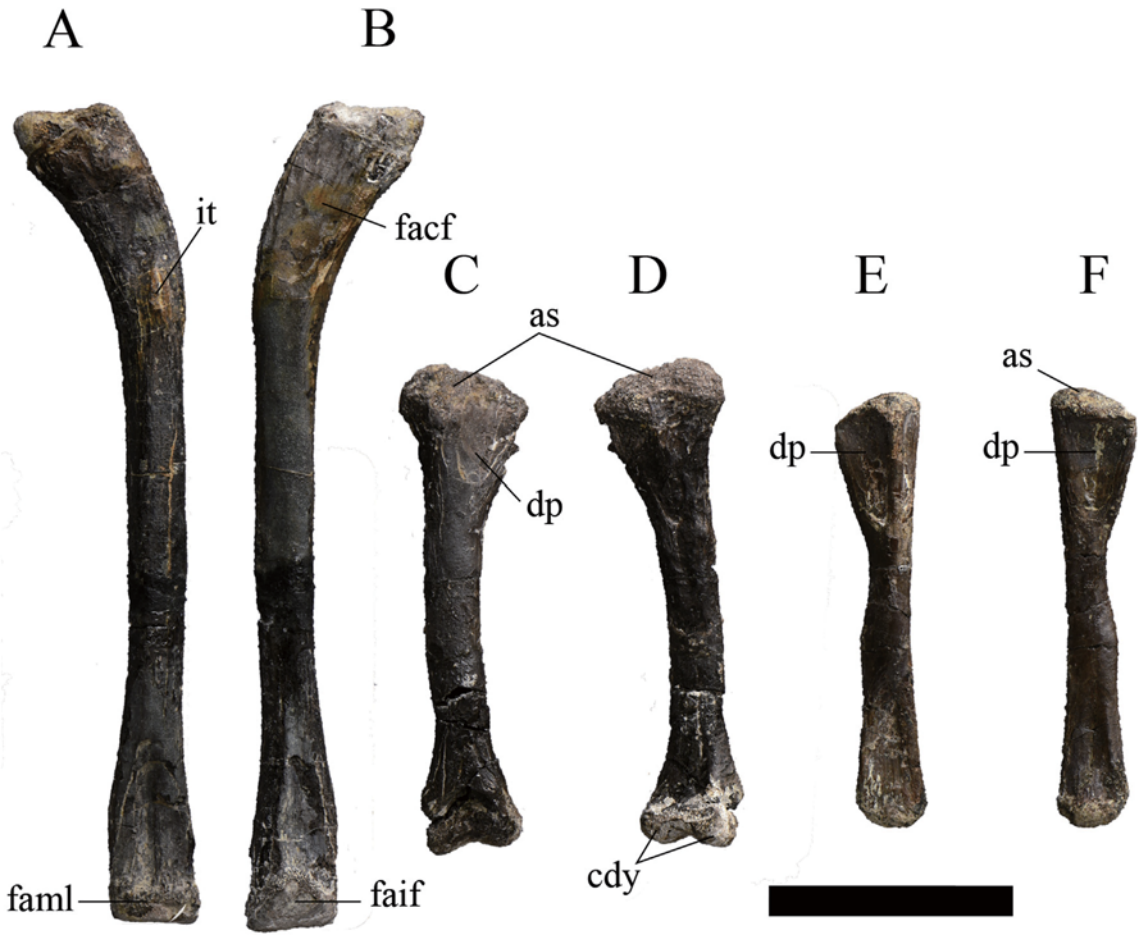

Fig. 14. Hindlimb elements of *Yanjisuchus longshanensis* gen. et sp. nov., holotype (YJDM 00009). Fibula in lateral (A) and medial (B) views. Right metatarsal II in ventral (C) and dorsal (D) views. Left metatarsal IV in lateral (E) and medial (F) views. Scale bar = 3 cm.

section. The dorsal surface is much smoother than the ventral surface. The distal condyles are well developed and the intercondylar furrow is moderately deep. A triangular fossa is present on the distal part of the dorsal surface. Shallow ligament pits are evident on the both sides of the distal end.

Left metatarsal IV is incomplete, with the distal articular end missing (Fig.14E and F). The identification of the bone is based on the presence of a depression on both the dorsal and ventral surfaces of the proximal portion, and on the relative length of the metatarsal. The proximal articular facet for a distal tarsal is triangular. The preserved part of the metatarsal is 55 mm long. The hatchet-shaped proximal portion is medially thin and laterally very thick. Shallow muscle striations are present on all surfaces of the proximal portion. A 13 mm long groove is present along the lateral edge of the proximal portion, presumably for articulation of the reduced metatarsal V. The shaft is medially concave and laterally straight. In dorsal view, a triangular depression similar to that seen on metatarsal II is present on the distal portion, and bears coarse muscle scars. In ventral view, a narrow depression or groove is present in the distal portion, with fine muscle scars. The distal end is incomplete, with the condyles for the first phalanx damaged.

5.4. Osteoderms

Four dorsal osteoderms are preserved (Fig. 15). The largest osteoderm is nearly complete, and is identified as a posterior dorsal (lumbar) osteoderm based on the morphological parameters used in *Itasuchus jesuinoi* (Marinho et al., 2006) and the similar ones for *Montealtosuchus arrudacamposi* (Tavares et al., 2015) (Fig. 15A). It is generally rectangular and wider (54.5 mm) than long (33.6 mm), whereas anterior dorsal osteoderms are greater in length than in width (Tavares et al., 2015). The dorsal surface bulges slightly and is covered in pits and ridges as in other neosuchians. There is no anterolateral process. The dorsal keel near the posterior edge is weak and evidently short, extending along the posterior third of the length of the osteoderm. The keel is situated slightly lateral to the dorsal midline. A strap-like smooth surface lies along the anterior edge. A shelf separating the smooth surface from the ornamented surface posteriorly suggests that the anterior osteoderms overlapped the posterior ones in life as in *M. arrudacamposi*. The positions of the overlapping surface and the dorsal keel indicate that this osteoderm was parasagittal and situated to the left of the neural spine in life. In addition, sutural facets are evident on both the medial and lateral sides of the osteoderms (Fig. 15E). This indicates that the osteoderm had a neighboring one to articulate with on each side, implying that the dorsal osteoderms were transversely arranged in more than two rows, probably similar to the condition in *Kansajsuchus extensus* (Kuzmin et al., 2018). The ventral surface of the osteoderms is concave and has several shallow pits. Some grooves along the posterior edge and others intersecting each other on the ventral surface may have been made during preservation.

A second osteoderm is incomplete (Fig. 15B), and morphologically similar to the cervical osteoderms of *S. djadochtaensis* (Pol

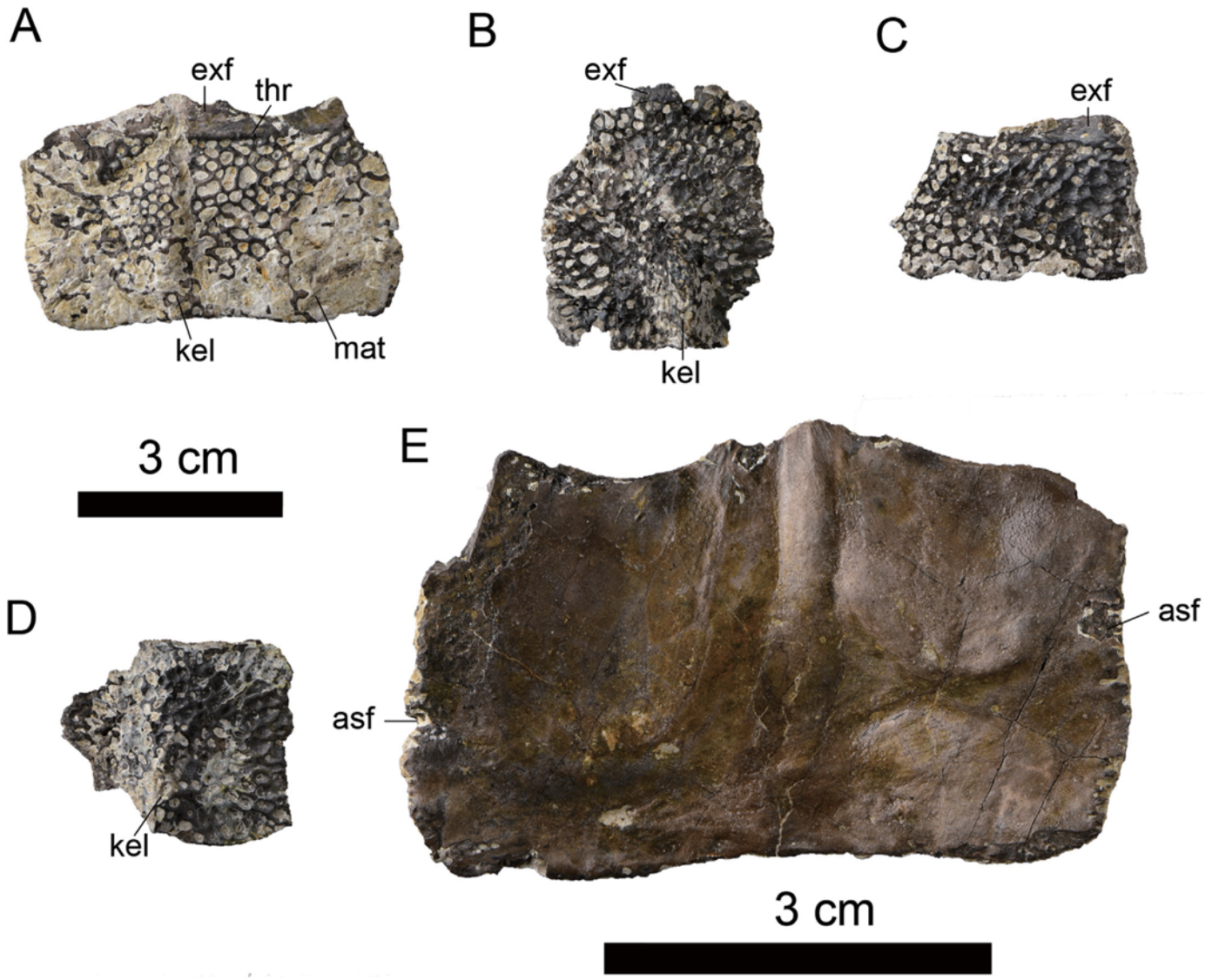

Fig. 15. Osteoderms of *Yanjisuchus longshanensis* gen. et sp. nov., holotype (YJDM 00009) in dorsal (A–D) and ventral (E) views. A, dorsal (lumbar) osteoderm; B, nuchal osteoderm; C, second dorsal osteoderm; D, dorsal (sacral) osteoderm; E, dorsal osteoderm depicted in (A), showing the articular facets for the medial and lateral neighboring osteoderms.

et al., 2009) in that a high lateral keel arises from the posterior edge. This is unlike *Sunosuchus junggarensis* (IVPP V10607), in which the keel dominates the entire length of the osteoderm (Wu et al., 1996a). Grooves and pits cover the entire dorsal surface. A small step of the smooth articulated area is preserved anteriorly. In cross-section, the osteoderm is folded at a 202° angle. Several shallow pits are present on the ventral surface. A sutural facets is only present along the medial side.

A third osteoderm is also incomplete, with most of the lateral part broken away (Fig. 15C). It is identified as a part of a dorsal osteoderm based on comparison with *S. djadochtaensis* (Pol et al., 2009). A lateral keel is present, arising from the posterior edge and dominating the posterior half of the bone as in the second osteoderm. Grooves and pits cover the dorsal surface, including the keel. Anteriorly, the smooth overlapping surface is evident, and a sutural facet is present along the medial side. In cross-section, the osteoderm is folded at a 202° angle. Several shallow foramina are visible on the ventral surface.

A fourth osteodermal fragment (Fig. 15D) presumably also came from a dorsal (sacral) osteoderm. A section of the overlapping surface is preserved along the anterior border as in the first and third osteoderms. Some shallow pits are present on the ventral surface, which is not as concave as in the cervical osteoderms.

6. Phylogenetic analyses and results

Before we can distinguish *Y. longshanensis* from other neosuchians and compare it with closely related taxa, we need to establish its phylogenetic position within Neosuchia. The data matrix used in our phylogenetic analysis was adapted from Kuzmin et al. (2018), which in turn was based on Turner (2015) and included most known paralligatorids. With the addition of *Y. longshanensis* and two recently described neosuchians, *Tarsomordeo winkleri* (Adams, 2019) and *Scolomastax sahlsteini* (Noto et al., 2019), the data matrix included 114 taxa and 324 morphological characters (see Electronic Supporting Material). In character scaling for included taxa, we used the revised version of Schwarz et al. (2017) for the included five atoposaurids, that of Adams (2019) for *T. winkleri*, and that of Noto et al. (2019) for *S. sahsteini*. Characters 95 and 207 were modified as in Adams (2019) and Noto et al. (2019), which also used phylogenetic data matrices derived from that of Turner (2015). For *Shamosuchus djadochtaensis*, we changed

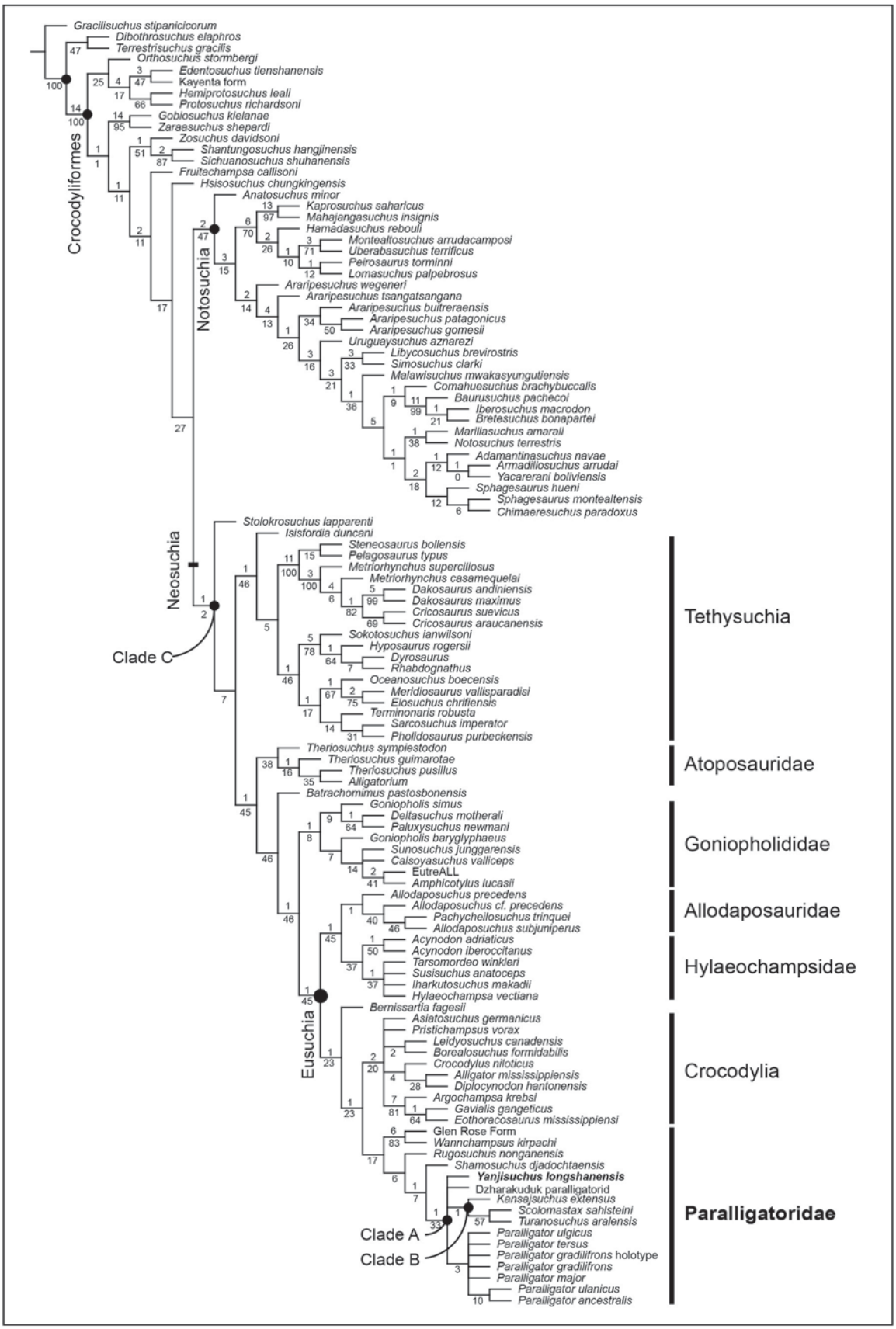

Fig. 16. Consensus of ten MPTs (Tree length = 1649 steps, CI = 0.243; RI = 0.668) recovered by the first phylogenetic analysis with 114 taxa and 321 characters, all unordered, depicting the phylogenetic relationships of *Yanjisuchus longshanensis* gen. et sp. nov., holotype (YJDM 00009). Bremer support values and bootstrap values are provided above and below each node, respectively showing limited support for clades of interest.

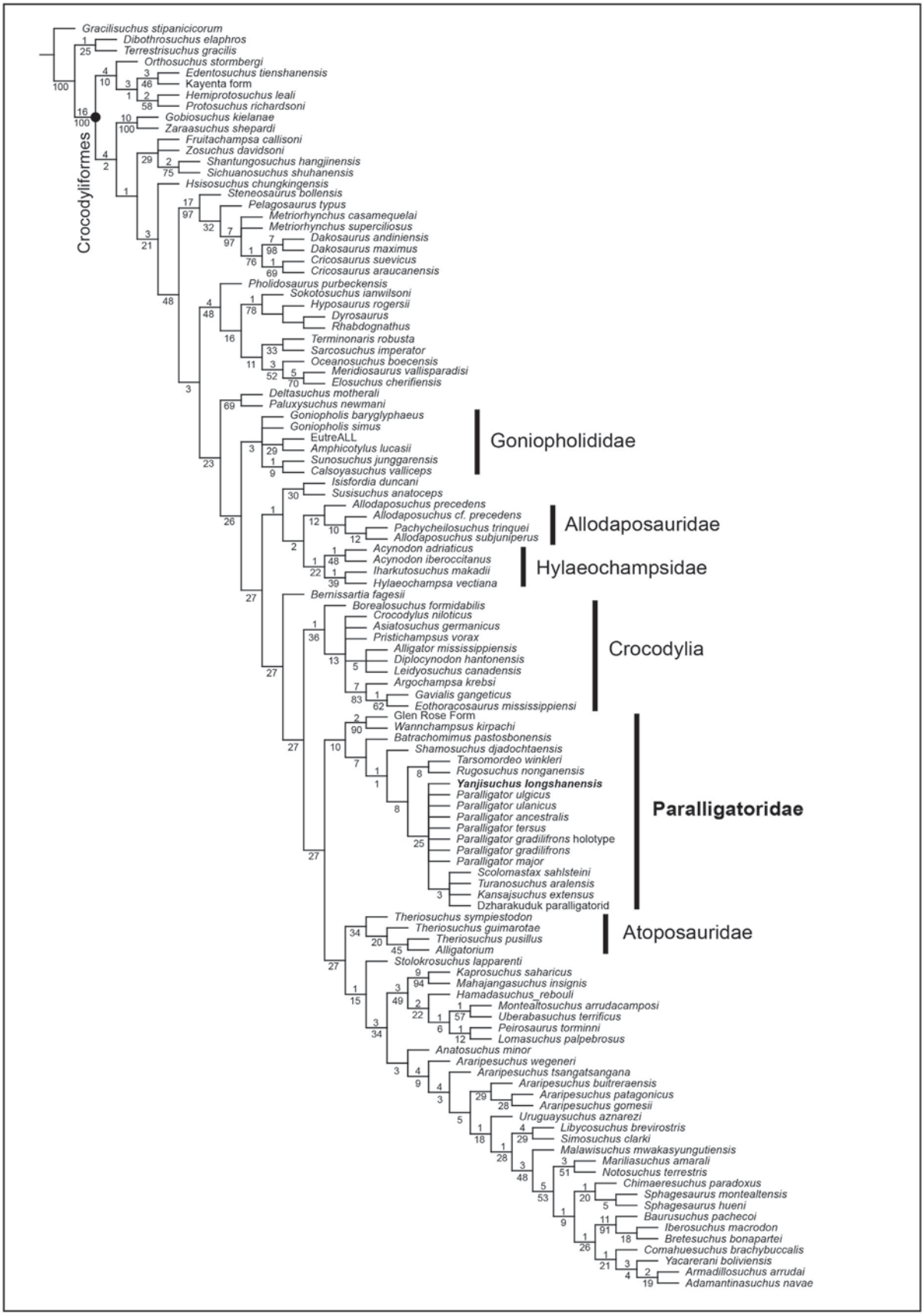

Fig. 17. Consensus of ten MPTs (Tree length = 1727 steps, CI = 0.232; RI = 0.678) was recovered by the second phylogenetic analysis with 114 taxa and 321 characters (33 additively ordered), depicting the phylogenetic relationships of *Yanjisuchus longshanensis* gen. et sp. nov., holotype (YJDM 00009). Bremer support values and bootstrap values are provided above and below each node, respectively showing limited support for clades of interest.

the score for character 59 from '?' to '0' because the ventral surface of the basisphenoid is clearly shorter than the basioccipital (see Turner, 2015: fig. 3C, F).

The data matrix was analyzed using TNT v.1.5 standard version (Goloboff and Catalano, 2016). *Gracilisuchus stipanicicorum* (Romer, 1972) was used as an outgroup as in previous studies related to Paralligatoridae, although Wilberg (2015) showed that using *Gracilisuchus* as the outgroup produced incorrect results, and that poposaurids were a better outgroup. We set the maximum of trees to 10,000, and 1000 replicates of Wagner trees (using random addition sequences) followed by tree bisection and reconnection (TBR) branch swapping (holding 10 trees per replicate). The data were analyzed using a Traditional Search strategy as in recent studies (Turner, 2015; Adams et al., 2017; Kuzmin et al., 2018; Noto et al., 2019; Adams, 2019). Considering differences in the treatment of characters and the inclusion of terminal taxa among the recent studies, we conducted two phylogenetic analyses. In the first analysis, we treated all characters as unordered as in Kuzmin et al. (2018), and in the second analysis, we treated 33 characters as having additively ordered multiple states as in Turner (2015), Adams et al. (2017); Noto et al. (2019), and Adams (2019). Moreover, we also excluded characters 5, 277, and 281 from our analyses as in the aforementioned studies.

The first analysis, with no character ordering yielded 10 most parsimonious trees (MPTs) with a tree length of 1649 steps, a consistency index (CI) of 0.243, and a retention index (RI) of 0.668. In the strict consensus of the 10 MPTs, *Y. longshanensis* was recognized as a paralligatorid but had an unresolved relationship with the Dzharakuduk paralligatorid, a clade including *K. extensus*, *S. sahlsteini*, and *T. aralensis*, and a clade including seven species of *Paralligator* (Fig. 16). The second analysis, with the 33 characters ordered, produced 10 MPTs with a tree length of 1727 steps, a consistency index (CI) of 0.232, and a retention index (RI) of 0.678. In the consensus of the 10 MPTs, *Y. longshanensis* was again recognized as a paralligatorid, but this time had an uncertain relationship with the seven species of *Paralligator* and a clade formed by the Dzharakuduk paralligatorid, *K. extensus*, *S. sahlsteini*, and *T. aralensis* (Fig. 17).

As both analyses posited the Glen Rose Form-*Wannchampsus kirpachi* clade as the sister group of the clade formed by all traditionally recognised paralligatorids, we treated the Glen Rose Form and *W. kirpachi* as two paralligatorids as in Adams (2014), Turner (2015), Adams et al. (2017), Noto et al. (2019), and Adams (2019). As a whole, the phylogenetic position of *Y. longshanensis* within the Paralligatoridae did not change much between the two analyses carried out in this study, but the relationships of the Paralligatoridae to other groups of the Metasuchia (*sensu* Benton and Clark, 1988) differed considerably (see below). In addition, the composition of the Paralligatoridae differed between the two analyses: the clade included 16 species in the first analysis, but 18 species in the second with the 33 characters ordered.

7. Comparison

7.1. Morphological comparison

The following comparisons mainly involve the 18 members of the Paralligatoridae recognized by the second analysis (Fig. 17). Although *Y. longshanensis* is not well preserved, its distinctive morphological features are obvious. It can be diagnosed mainly based on features from the frontal, jugal (Figs. 3, 4, 7) and dentary fragment (see above) and is morphologically distinguishable from other paralligatorids.

W. kirpachi and the Glen Rose Form forms the sister-group to other Paralligatoridae. Adams (2014) suggested that the two were referable to the same genus. Since the Glen Rose Form has not been described, we used *W. kirpachi*, which is from the upper Lower Cretaceous (late Aptian) of Texas, USA, for comparison with *Y. longshanensis*. Its frontal lacks midline and preorbital ridges (Adams, 2014: fig. 2.2), in contrast to the presence of the two ridges in *Y. longshanensis*.

Batrachomimus pastosbonensis Montefeltro et al., 2013 from the Upper Jurassic of Brazil is closer to other paralligatorids than are *W. kirpachi* and the Glen Rose Form. The preserved frontal differs from that of *Y. longshanensis* in that it does not have a preorbital ridge and midline ridge on the dorsal surface.

Shamosuchus djadochtaensis from the Upper Cretaceous of Mongolia (Campanian, Dashzeveg et al., 2005), is closer to the remaining paralligatorids than is *B. pastosbonensis*. *Y. longshanensis* is distinguishable from *S. djadochtaensis* in that the jugal forms the entire ventral margin of the infratemporal fenestra, the interorbital width is much greater than the interfenestral width, and the dentaries are fused (see Turner, 2015: fig. 3).

The *Tarsomordeo winkleri-Rugosuchus nonganensis* clade is closer to the remaining paralligatorids than is *S. djadochtaensis*. *T. winkleri* is from the Lower Cretaceous (Aptian) of Texas (Adams, 2019), and *R. nonganensis* from the Upper Cretaceous (Santonian) of Jilin, China. The preserved mandible of *T. winkleri* shows that there is no diastema and the dentaries are not fused, unlike in *Y. longshanensis*. The lack of a preorbital ridge and a diastema as well as the paired dentaries, separate *R. nonganensis* from *Y. longshanensis*.

In phylogenetic position, following the *Tarsomordeo winkleri-Rugosuchus nonganensis* clade are a group of *Y. longshanensis* and seven species of *Paralligator* with uncertain relationships as well as a clade formed by the remaining four paralligatorids. Turner (2015) argued that his review of all species referred to *Paralligator* (his *Shamosuchus*) recognized three valid taxa: *Shamosuchus djadochtaensis*, *P. gradilifrons*, and *P. major*. Therefore, *Y. longshanensis* was compared only with the three species. Comparison with *S. djadochtaensis* was made earlier. *P. major* is from the Upper Cretaceous (Santonian) of Mongolia (Turner, 2015). Comparison between *Y. longshanensis* and *P. major* is limited because few corresponding structures are available. *P. major* is a very large animal, which might be the only feature distinguishing this species from *Y. longshanensis* and from the other species of *Paralligator* (Turner, 2015). In addition, the interorbital breadth of the frontal is much greater than the interfenestral width of the supratemporal in *Y. longshanensis*, while the former is only slightly broader than the latter in *P. major* (see Turner, 2015: fig. 5A).

P. gradilifrons was discovered from the Upper Cretaceous (Cenomanian through Santonian, Dashzeveg et al., 2005) of Mongolia. This species evidently differs from *Y. longshanensis* in having paired dentaries, no diastema of the dentary, a short mandibular symphysis, and an interfenestral width of the parietal that is nearly as great as the width of the interorbital region (Turner, 2015: fig. 5E-H). On the other hand, *Y. longshanensis* is comparable with *P. gradilifrons* in having midline ridge and preorbital ridges on the frontal.

Grouped with the polytomy of eight species is the clade formed by four species with uncertain relationships: *S. sahlsteini*, *Turanosuchus aralensis*, *K. extensus* and the Dzharakuduk paralligatorid. *S. sahlsteini* from the Upper Cretaceous (Cenomanian) of the USA is fragmentary, but the preserved dentary shows no fusion with the opposite element, no diastema anteriorly, and a very short mandibular symphysis (Noto et al., 2019: fig. 2). These are very different from *Y. longshanensis*. *T. aralensis* was based on skull fragments from the Upper Cretaceous (Santonian) of Kazakhstan (Efimov, 1988; Halliday et al., 2015: fig. 11). With the dentaries unfused and no diastema posterior to the fourth dentary tooth, *T. aralensis* is evidently different from *Y. longshanensis*. *K. extensus* is

represented by many isolated bones from the Upper Cretaceous (Santonian) of Tajikistan, of which many are incomplete (Efimov, 1975). If we consider the referred specimens, *K. extensus* can be distinguished from *Y. longshanensis*. In *K. extensus*, the referred frontal does not have a preorbital ridge and the referred left femur has the fourth trochanter relatively distally positioned (see Halliday et al., 2015: fig. 10B). The ratio between the length of the proximal portion (from the proximal end to the midpoint of the trochanter) and the total length of the femur is 0.388, in contrast to about 0.34 in *Y. longshanensis*. Fragmentary specimens of a large neosuchian from the Upper Cretaceous (Turonian) of the Dzharakuduk locality, Uzbekistan, are known as the Dzharakuduk paralligatorid (Kuzmin et al., 2018). It is difficult to compare *Y. longshanensis* with the Dzharakuduk paralligatorid due to the fragmentary nature of the specimens. According to the character matrix of Kuzmin et al. (2018), the splenial makes a large contribution to the mandibular symphysis in the Dzharakuduk paralligatorid, whereas the bone is not involved in the symphysis in *Y. longshanensis*.

P. sungaricus is also from Jilin Province and was originally classified as a paralligatorid (Sun, 1958). The Nenjiang Formation that produced *P. sungaricus* is about 15 million years younger than the Longjing Formation, which yielded *Y. longshanensis*, and the fossil locality is about 100 km from where *Y. longshanensis* was collected. *P. sungaricus* is very fragmentary, being represented by four dorsal vertebrae with dorsal osteoderms and referred specimens that constitute an incomplete femur and tibia. This species was excluded from our phylogenetic analyses, as in other studies, due to its uncertain status (see Turner, 2015). The preserved elements are not distinguishable from those of other *Y. longshanensis*.

7.2. Phylogenetic comparison

Most recent paralligatorid phylogenetic analyses were based on a data matrix derived from Turner (2015), and all but Kuzmin et al. (2018) included only two species of *Paralligator* (*P. gradilifrons* and *P. major*) in the phylogenetic analysis due to the uncertain status of the other four species referred to the genus (Turner, 2015). Recent studies (such as Adams et al., 2017; Noto et al., 2019; Adams, 2019) used a Traditional Search in TNT (Goloboff and Catalano, 2016) with the same settings, and the same additive ordering of 33 characters, as the analysis of Turner (2015). In the Kuzmin et al. (2018) analysis, the data matrix was also derived from Turner (2015) but had an additional six paralligatorid taxa, including the four uncertain species of *Paralligator*, the *P. gradilifrons* holotype (treated as an individual taxon), and the Dzharakuduk paralligatorid. Kuzmin et al. (2018) analyzed the data with the same search method and settings as in the aforementioned studies left all characters unordered as in our first analysis.

In comparison with Kuzmin et al. (2018), the results of our first analysis with the same search method and same settings are similar in that all seven species of *Paralligator* formed a monophyletic grouping within the Paralligatoridae, but differ in the placement of Paralligatoridae with respect to other major groups within Neosuchia (Fig. 16). In Kuzmin et al. (2018), the monophyly of the Eusuchia was not recognized and the Paralligatoridae-Atoposauridae clade, Crocodylia, and Goniopholididae formed a set of successively close outgroups to Tethysuchia (Kuzmin et al., 2018: fig. 21), while the Tethysuchia, Atoposauridae, Goniopholididae, Hylaeochampsidae-Allodaposuchidae clade, and Crocodylia formed a set of successive sister-groups towards the Paralligatoridae in our first analysis. Alternatively, these clades and the Paralligatoridae formed a set of successive sister-groups towards the Crocodylia. In the analysis of Kuzmin et al. (2018), the Glen Rose Form-*Wannchampsus kirpachi* clade was also grouped together with the Atoposauridae and the Hylaeochampsidae, and Allodaposuchidae were recovered in a more basal position than other neosuchian groups. *B. pastosbonensis* was often considered a paralligatorid in studies that included this taxon (such as Montefeltro et al., 2013; Turner, 2015) but was excluded from the Paralligatoridae both in our first analysis and by Kuzmin et al. (2018), as it was positioned as a successive taxon from Atoposauridae. It was also noticeable that in this analysis that *Tarsomordeo winkleri* no longer forms sister taxon of the clade *Rugosuchus nonganensis* + *Paralligator major*, as in its original analysis of Adams (2019), rather, it is retrieved as a member of Hylaeochampsidae.

Our second analysis followed Turner (2015), Adams et al. (2017), Noto et al. (2019), and Adams (2019) with respect to search method, and data settings, and ordering of the 33 characters. The results obtained by our second analysis are comparable to those of the aforementioned studies in that the monophyly of the Paralligatoridae was confirmed, although many more species were included. However, our results were very different from those of previous studies with respect to the position of Paralligatoridae within the Neosuchia (Fig. 17). The most striking of the differences was that the Neosuchia was not recognized as monophyletic clade, but rather was broken into a set of successive sister-groups towards the Notosuchia. It is true that varying interrelationships within the Neosuchia or the Eusuchia have been recovered by recent studies on paralligatorids, but the monophyly of the Neosuchia was consistently recognized in those studies. Although the results obtained by our second analysis with the 33 characters ordered differed considerably from those of the aforementioned studies on paralligatorids, the results of our first analysis were less unusual. In these studies, the Tethysuchia, Pholidosauridae, and Goniopholididae were posited as a set of successive sister-groups towards the Eusuchia that included the Hylaeochampsidae-Allodaposuchidae clade, Crocodylia, and the Paralligatoridae with consist largely of polytomies (Fig. 17). In our first analysis, the monophyletic Eusuchia formed by these same three clades, and Crocodylia and Paralligatoridae were resolved as the sister taxa. Also, in this analysis, we recovered *B. pastosbonensis* and *T. winkleri* as paralligatorids. The phylogenetic topology obtained by our first analysis were also better supported than those of our second analysis in terms of the relatively higher values of the Bremer (Bremer, 1994) and bootstrap (Efron, 1979) supports for the relevant clades (Figs. 16, 17). Therefore, we use the results of the first analysis as the basis for the following discussion.

8. Paleobiogeography

Noto et al. (2019) mentioned that our knowledge of paralligatorid distribution and evolution is clouded by disagreement across studies with respect to the phylogenetic position of the Late Jurassic *B. pastosbonensis* of South America. As mentioned earlier, our two analyses also showed such an inconsistency. For the paralligatorid status of *T. winkleri* from Texas, our study also showed a controversial conclusion. Therefore, whether *B. pastosbonensis* or *T. winkleri* are referrable to the Paralligatoridae needs further study.

Our two phylogenetic analyses both suggested that the Glen Rose Form and *W. kirpachi* from Texas were the basal most members of the Paralligatoridae. In addition to our study, at least five recent studies considered the two Texan forms as paralligatorids although their placement within the family was not consistent (Adams, 2014; Turner, 2015; Adams et al., 2017; Noto et al., 2019; Adams, 2019). Therefore, our study supports the view that the Paralligatoridae is a diverse clade, with a wide distribution in the northern hemisphere and a time range from the late Early Cretaceous to the Late Cretaceous (see Fig. S1 in Electronic Supporting Material). However, it is too early to comprehensively evaluate the origin and evolution of the Paralligatoridae, because recent

studies have not yet found a relatively stable phylogenetic pattern either inside or outside the family.

9. Discussion

Our morphological knowledge of *Y. longshanensis* is limited due to the incompleteness of the specimens available. However, *Y. longshanensis* can be diagnosed by a set of derived characters from the frontal, jugal, dentary, fibula, and osteoderms. The most significant of those diagnostic traits include the wedge-shaped elevation of the frontal anteriorly, the elongate posterior process of the jugal, and the fused dentaries with a diastema posterior to the fourth dentary tooth.

As mentioned earlier, the results of the first analysis appeared more comparable to those of other recent studies and are used here to detail the internal relationships of the Paralligatoridae. The paralligatorid status of *Y. longshanensis* was supported by eight unequivocal synapomorphies. They included characters 56 (0), 59 (0), 66 (0), 170 (1), 219 (2), 297 (1), 311 (1), and 320 (1), but only characters 59, 170, and 297 are preserved in *Yanjisuchus*. Within the Paralligatoridae, *Y. longshanensis* was successively crowner in phylogenetic position than Glen Rose Form-*Wannchampsus kirpachi* clade, *R. nonganensis*, and *S. djadochtaensis* based on different sets of unequivocal synapomorphies, respectively (see Electronic Supporting Material). Furthermore, *Y. longshanensis* was recovered within a polytomous clade (Fig. 16. Clade A) supported by seven unequivocal synapomorphies, including characters 56 (1) – basisphenoid is virtually excluded from the ventral surface by the pterygoid and basioccipital, 69 (2) – choanal groove is completely septated, 92 (0) – cervical vertebrae are amphicoelous or amphiplatyan, 93 (0) – trunk vertebrae are amphicoelous or amphiplatyan, 107 (1) – presence of unsculptured region along the alveolar margin on the lateral surface of the maxilla, 265 (1) – anteromedial corner of the supratemporal fenestra is smooth, and 267 (0) – capitate process of the laterosphenoid is laterally oriented. Of these synapomorphies, only characters 92, 93 and 265 are preserved in *Yanjisuchus*. Within Clade A, 10 MPTs indicated that *Y. longshanensis* might have had a sister-group relationship with the Dzharakuduk paralligatorid, and that these paired taxa might have been closely related to Clade B, which included a *Turanosuchus aralensis-Scolomastax sahlsteini* clade positioned as sister to *K. extensus*. All these taxa might in turn have formed a clade constituting the sister-group of *Paralligator* (see Electronic Supporting Material: Fig. S2).

Although the phylogenetic relationships of paralligatorids and other major groups within Neosuchia are better resolved by our first analysis than the second, such relationships were weakly supported even in the first analysis. For most clades either within or outside Paralligatoridae, Bremer support was no greater than '1'. The bootstrap support values were similarly low (Fig. 16). Therefore, it will not be surprising if different phylogenetic relationships within Paralligatoridae and/or among neosuchian groups are altered when either new taxa or better specimens of *Y. longshanensis* and other fragmentary taxa become available.

Some recent studies have considered Paralligatoridae to be restricted to the Cretaceous of Asia, ranging from Tajikistan, Kazakhstan through Mongolia to Eastern China (Turner, 2015; Kuzmin et al., 2018). With the emergence of taxa from outside Asia, the clade had to be acknowledge as having a much wider geographic range. As suggested by phylogenetic studies incorporating *T. winkleri* and *S. sahlsteini* from Texas, USA, the Asian paralligatorids did not form a monophyletic group (Noto et al., 2019; Adams, 2019), which implied a very different scenario for the origin and evolution of the Asian taxa from that suggested by the studies of Turner (2015) or Kuzmin et al. (2018). Moreover, the discovery of *Y. longshanensis* made the scenario further complicated. Therefore, it is too early to discuss these issues before a stable phylogenetic pattern can be reached.

10. Conclusions

We concluded that *Y. longshanensis* is a new genus and species. It most specialized characteristics are a frontal with a wedge-shaped elevation anteriorly and fused dentaries with a diastema posterior to the fourth tooth. Phylogenetically, *Y. longshanensis* might be closely related to the Dzharakuduk paralligatorid. The internal relationships of the Paralligatoridae and the phylogenetic relationships among neosuchian groups were resolved by our study, but supporting values for most clades were very low. Therefore, it will be necessary to find new taxa or better specimens of fragmentary taxa in order to verify the phylogenetic pattern obtained here for the Neosuchia and propose a comprehensive scenario for the origin and evolution of the Paralligatoridae. The discovery of *Y. longshanensis* certainly provides further information on the taxonomic diversity of the Paralligatoridae and enriches the local archosaur fauna of the Yanji Basin.

Acknowledgements

The authors would like to thank the Yanji Municipal Bureau of Land and Resources, Yanji Paleontological Research Centre and Yanji Dinosaur Museum for allowing us to conduct excavation and research. We are grateful to all field team members and other staff who took part in the work for long hours. We thank Mr. Lishi Xiang and Ms. Renfang Cao of IVPP for fossil preparation. We thank Mr. Hailong Zang of IVPP for photographic work. We acknowledge the use of the program TNT, which is made available through the Willi Hennig Society. Lastly, we would like to extend our gratitude to the journal's chief editor, Eduardo Koutsoukos, reviewer Corwin Sullivan and another anonymous reviewer for their constructive comments and feedbacks on the manuscript. This work was supported by the Natural Science Foundation of China – Grant No. NSFC 41688103, a grant from the Yanji Paleontological Research Centre, and a research grant from the Canadian Museum of Nature.

References

Adams, T.L., 2014. Small crocodyliform from the Lower Cretaceous (Late Aptian) of Central Texas and its systematic relationship to the evolution of Eusuchia. Journal of Paleontology 88, 1031–1049.

Adams, T.L., 2019. Small terrestrial crocodyliform from the Lower Cretaceous (late Aptian) of Central Texas and its implications on the paleoecology of the Proctor Lake Dinosaur locality. Journal of Vertebrate Paleontology 39, 1031–1049. https://doi.org/10.1080/02724634.2019.1623226.

Adams, T.L., Noto, C.R., Drumheller, S., 2017. A large neosuchian crocodyliform from the Upper Cretaceous (Cenomanian) Woodbine Formation of North Texas. Journal of Vertebrate Paleontology 37 (4). https://doi.org/10.1080/02724634.2017.1349776.

Benton, M.J., Clark, J.M., 1988. Archosaur phylogeny and the relationships of the Crocodylia. In: Benton, M.J. (Ed.), The phylogeny and classification of the tetrapods, Vol. 35A. Clarendon Press, Oxford, p. 295e338. Systematics Association Special.

Bohlin, B., 1953. Fossil reptiles from Mongolia and Kansu. Reports from the scientific expedition to the north-western provinces of China under leadership of Dr Sven Hedin. Statens Etnografiska Museum, Stockhom.

Bremer, K., 1994. Branch support and tree stability. Cladistics 10 (3), 295–304.

Brochu, C., Parris, D.C., Grandstaff, B.S., Denton JR., R.K., Gallagher, W.B., 2012. A New Species of Borealosuchus (Crocodyliformes, Eusuchia) from the Late Cretaceous—Early Paleogene of New Jersey. Journal of Vertebrate Paleontology 32, 105–116.

Buscalioni, A.D., Sanz, J.L., 1990. The small crocodile *Bernissartia fagesii* from the Lower Cretaceous of Galve (Teruel, Spain). Bulletin de l'Institut Royal des Sciences Naturelles de Belgique, Sciences de la Terre 60, 129–150.

Carroll, R., 1988. Vertebrate paleontology and evolution. W. H. Freeman, New York, p. 698.

Clark, J.M., 1986. Phylogenetic relationships of the crocodylomorph archosaurs [Unpubl. PhD thesis]. University of Chicago, p. 556.